Final point-by-point response to the reviews and a list of all relevant changes

S. ZHU[1], K.N. Sartelet[1], and C. Seigneur[1]

[1]CEREA, joint laboratory Ecole des Ponts ParisTech - EDF R&D, Université Paris-Est, 77455 Champs-sur-Marne, France.

The authors thank all referees for providing thorough reviews and thank top editors for their efforts to improve this paper. Here, we offer a final point-by-point response to both of the referees, follow by a list of all relevant changes and a marked-up manuscript version.

1 Final response to Anonymous Referee 1

The authors thank the referee for providing a thorough review. We modified and clarified the paper as suggested. Each item starts with the reviewer's comment in italics.

1.1 Major Comments

• *The new model has the ability to resolve aerosol mixing state in great detail, but at a significant computational cost. Thus the following two questions must be addressed. What aspects of mixing state are important to capture in a model or simulation? How should the mixing state representation (i.e., the specific species groups and bin boundaries for the composition fractions) be designed to efficiently capture this information? Unfortunately, the paper has almost nothing to say about these questions. For the second test case (Paris), there is no discussion of why the particular species groupings and composition bin boundaries were chosen. The abstract mentions investigating the importance of representing mixing state (P. 7938, L. 8-10), but the results in Section 4 simply demonstrate the external mixing of the aerosol and do not discuss why it is important. The size distributions and the mass concentrations of secondary aerosol species do not differ much between the internal and external mixing simulations. Aerosol properties that could be sensitive to mixing state (e.g., CCN and optical properties) are not discussed. Some discussion of these issues is needed, and would be of greater interest to readers than, for example, some of the material in Section 2.*

This paper aims at presenting the model. Therefore, we tried to keep the model description as general as possible, so that the model can easily be applied to different applications. An example of application is given here, focusing on showing that aerosols may not be totally mixed in urban areas and how different aerosol processes (condensation/evaporation, coagulation) impact the mixing state. The

mixing state representation is flexible enough to be modified by users and it would particularly affect CCN and optical properties. A discussion about the importance of the mixing state for CCN and optical properties is given in the introduction "The mixing state assumption may strongly influence aerosol chemistry and the hygroscopic characteristics of particles. Particles from different origins may not be well mixed, and their chemical composition may vary with their origins, leading to variations in their hygroscopic characteristics. This chemical identity of particles is gradually lost as the degree of mixing increases (or completely lost under the internal mixing assumption). By influencing the hygroscopic characteristics of particles, the mixing state also influences the formation of secondary organic aerosols (SOA), because condensation/evaporation differs for species that are hydrophilic and/or hydrophobic (Couvidat et al., 2012). As the particle wet diameter is strongly related to the hygroscopic properties of particles, the mixing state also impacts particle wet diameters and the number of particles that become Cloud Condensation Nuclei (CCN), because the activation of particles into CCN is strongly related to the particle wet diameter (Leck and Svensson, 2014). By influencing CCN, the mixing state also affects aerosol wet removal and thus the aerosol spatial/temporal distribution. Besides, the mixing state influences the particle optical properties, which depend on both the particle size distribution (wet diameters) and composition (different chemical species possess different absorption/scattering properties). Lesins et al. (2002) found that the percentage difference in the optical properties between an internal mixture and external mixture of black carbon and ammonium sulphate can be over 50% for wet aerosols. The mixing state may also influence radiative forcing, as shown by Jacobson (2001) who obtained different direct forcing results between external and internal mixing simulations of black carbon."

Concerning the particular species grouping, a simple explanation is given in (P.7958,L.12): these species were grouped into 5 groups based on their chemical nature. Additional explanations are now added. "these species were grouped into 5 groups based on their chemical nature, which influences the formation of particles and their optical properties. Black carbon, organic species, inorganic species and dust are separated. Although sulphate could be separated from nitrate and ammonium for optical properties or for comparisons to observations of mixing state (Healy et al., 2012), and although chloride and sodium could be grouped together in a marine environment, all inorganic species are grouped together here for the sake of simplicity. However, because the hydrophilic properties of the particles strongly influence their formation and cloud condensation nuclei, hydrophilic and hydrophobic organic species are separated." The composition bin boundaries were chosen in order to balance the computational cost and the comprehensive representation of mixing state. These sections are designed to represent poor, medium and high abundance of one group within a particle.

The sentence in the abstract "The importance of representing the mixing state when modelling atmospheric aerosol concentrations is investigated in a box model simulation using data representative of air pollution in Greater Paris." was poorly formulated and is therefore rewritten as "The degree of mixing of particles is investigated in a box model simulation using data representative of air pollution in Greater Paris. The relative influence on the mixing state of the different aerosol processes (condensation/evaporation, coagulation) and of the algorithm used to model condensation/evaporation (bulk equilibrium, dynamic) is studied."

As the application presented in this paper is a 0D test, the information obtained from the simulation is insufficient to precisely discuss the importance of mixing state on AOD or CNN. We are currently coupling SCRAM to a 3D eulerian chemical transport model, and such discussion will be based on our future 3D simulation results.

•*In the model description section where the number and mass conservation equations are derived, the mass fraction of the last species (with index c) does not appear, since it is determined by the other (c-1) mass fractions. However, in the model implementation, when the composition bin boundaries are selected, it is possible to include this last mass fraction. Consider, for example, the first composition bin in Table 1, for which the mass fractions of HLI, HLO, HBO, and BC are all 0-20%. This composition bin could be subdivided into bins with DU mass fractions of 0-20, 20-80, and 80-100%. This might be desirable, depending on the rationale for selecting the composition bins. Incorporating this last mass fraction into the conservation equations (5-8) might be difficult or impossible. However, as discussed below, the C/E solver and the moving center scheme used for redistribution of particles in composition space do not directly use the conservation equations, and subdividing the bins to also reflect the DU mass fraction should not cause any difficulties for either. The authors should at least discuss how this is possible, even if the current model does not have this capability.*

In our model, we chose to compute the mass fraction of one of the group by mass conservation, i.e. the mass fraction of one group is not treated explicitly in the subdivision of the mass composition bins. In our example, we chose dust to be the group for which mass fraction is not treated explicitly, but if it is desirable to include the mass fraction of dust explicitly into the mass composition bins, another group could be chosen as the group for which mass fraction is not treated explicitly. This is now added in the paper. "Note that although as an example we chose dust to be the group for which mass fraction is not treated explicitly, another group could be chosen as the group for which mass fraction is not treated explicitly." Sentences are also added to the paper to explain how it would be possible to subdivide the mass fraction of every group. "If all groups need to have their mass fraction treated explicitly, additional composition bins for the last group should be added to the current composition list without any modification to the main structure of the program. The mass fraction of the last group would still be obtained by mass conservation, and the composition bin of the particles would be chosen depending on this mass fraction."

•*2993-10:The purpose of and need for the derivations and equations in Section 2.1.3 is not clear. These derivations are for a moving (Lagrangian) size-composition bin structure. However, the model is designed for application in chemical transport models that require a fixed size-composition bin structure. Thus equations 9-16 do not seem relevant here. Even if these equations were replaced by their fixed bin equivalents, they would not seem very relevant to the SCRAM model for the following reason. The conservation/ evaporation calculations for a time step involve solving (integrating) a set of ordinary differential equations for the time step. The particles in each size-composition bin are treated as uniform in size and composition, and the solver calculates their sizes and compositions some tens of seconds later, taking*

into account activity coefficients, particle phases (liquid/solid/mixed), equilibrium vapour pressures, mass transfer coefficients, etc. (The bulk equilibrium and hybrid approaches provide similar results using different assumptions and numerical methods.) The new size/composition information is then used by the size and composition redistribution algorithms to move particle number and species masses between bins, to reflect their new sizes and compositions. The conservation equations (5 and 8) have flux divergences on their right-hand sides, representing the next fluxes of number and mass into a bin. The moving diameter (or moving center) algorithm for composition (which numerically is probably the simplest algorithm that one could devise), does not use fluxes or flux divergences. The algorithm is consistent with the conservation equation (8) in some sense, but the algorithm. does not utilize the equation at all, and the equation is not needed to understand the model. If the authors feel that the discretized equations (fixed-bin versions) should remain the paper, then they should be in an appendix, although my recommendation is to remove them.

Either eulerian (fixed bins) or lagrangian (moving bins) approaches can be used to solve condensation/evaporation equations. However, the drawback of the eulerian approaches is numerical diffusion (see [Kim and Seinfeld(1990)]). That is why lagrangian approaches are commonly used, as in our model (instead of a fixed-bin eulerian approach). Equations 9-16 are crucial as they explain the derivation of the equations which are actually solved: equations (14) and (17). Because we use a lagrangian approach, a redistribution scheme onto a fixed-sections grid is necessary for 3D applications. The redistribution is applied after solving condensation/evaporation. The redistribution does not solve equations (5) and (8), it simply redistributes mass and number onto fixed sections. The redistribution algorithm is completely independent from the lagrangian solver, and the 0D model is operational without it. Equations (5) and (8) are continuous equations. They cannot be solved as they are: they have to be discretized. We use a sectional discretization. The discretization is explained in this paper as well as the derivation of the discretized equations from the continuous ones. As suggested by the reviewer, the derivation of the discretized equations is now put in an appendix. But the discretized equations (now 11 and 12) are kept, as those are the equations solved in the model. For clarity, the following explanation is added before section 2.1.1:"A lagrangian approach is used to solve the equations of change for the mass and number concentrations, which are redistributed onto fixed sections through a redistribution algorithm (moving diameter)."
Section 2.3 is moved to 2.1.5, so that all the algorithm for solving dynamic C/E are now detailed in section 2.1. Section 2.2 presents the simplified approaches that may be used to solve condensation/evaporation and to gain CPU time (bulk equilibrium, hybrid approaches).

•*2994-5: The condensation only test in Section 3 appears to be using a lagrangian bin structure, given the description of the test ("redistribution is not applied") and the near-exact agreement with the reference solution (which uses 500 lagrangian bins). Since the model is designed for CTMs that require a fixed bin structure, this is not a very appropriate test. A better test would use fixed bins, both with very high resolution for composition (e.g., 100 composition bins) and coarser resolution (10 and 3-5 bins). A high-resolution lagrangian-bin externally-mixed simulation could act as a reference for these fixed bin simulations. For comparison of the*

fixed bin and lagrangian bin results, plots like Figure 4 could be used, although they only provide a visually semi-quantitative comparison. Plotting the means and the standard deviations of the sulphate (i.e., species 1) mass fraction as functions of particle diameter would provide more quantitative comparison.

Because this paper presents an algorithm to solve condensation/evaporation for externally mixed particles, it is important to show the behaviour of this algorithm without redistribution. The impact of using different redistribution algorithms on mass and number concentrations has been investigated for example by Devilliers et al. (2013) who compared different algorithms for size section redistribution. They found that the moving diameter approach is one of the best performing algorithms. Furthermore, for mass fraction redistribution, a moving mass fraction approach similar to the moving diameter approach is the most appropriate one to use. Therefore, we do not need to compare different algorithms for mass fraction redistribution and we eel that it is appropriate to use the moving diameter approach. We agree that it is interesting to investigate the impact of different composition resolutions to external mixing results. So we conducted additional tests with 2 and 100 composition sections and compared their size distributions using the mean and standard deviation of sulphate mass fractions as suggested. The following discussion was added to the second paragraph of section 3:

"In order to investigate the influence of the composition resolution on simulation results, two additional tests are conducted using 2 and 100 composition bins. The mean mass fraction of species 1 is computed for all particles within each size section, as well as their standard deviations. Figure 3 shows the size distribution of these statistics. The mean mass fraction is barely affected by the different composition resolutions as the condensation rate of sulphate is independent of the particle compositions. However, a different composition resolution does lead to different standard deviation distributions, as only particles with larger fraction difference ($d > 0.2\mu m$ for 2 compositions and $d > 0.09\mu m$ for 10 compositions) can be distinguished from each other under coarser composition resolutions."

We also tried to plot the result composition distribution of the test with 100 composition sections using the style of figure 4. However the overall trend of the distribution is very similar to the 10 composition plot. Therefore, this figure would not add any interesting information to the paper and we think that it is better not to include it in the paper.

•*2994-19: The discussion in Section 4 suffers in numerous places from insufficient details about actual compositions in the size-composition bins that are discussed. The composition ranges for many of the composition bins are very wide (e.g., 20-80%). Without stating actual compositions (i.e., actual mass fractions of relevant or dominant species groups), the discussions end up being qualitative and somewhat vague. Providing more quantitative information (where appropriate) would strengthen and clarify the explanations of various mixing state features and behaviours.*

The composition range is chosen in order to balance the computational cost and the comprehensive representation of mixing state. These sections are designed simply to represent poor, medium and high abundance of one group within a particle. As suggested by the reviewer, we have added the actual mass fraction of each species groups during the discussion of section 4, which helps improve the presentation of

mixing state.

1.2 Other Comments

•*2994-25: P. 7939, L. 14-18. Add that by influencing CCN, the mixing state also affects aerosol wet removal and thus the aerosol spatial/temporal distribution.*

Thank you for your suggestion, we have added this description into the discussion of the mixing state importance in the fourth paragraph of the introduction.

•*Paragraph starting on P. 7939, L. 21. For completeness, include some modal aerosol models such at Stier et al. (2005, Atmos. Chem. Phys., p. 1125-1156) and Bauer et al. (2008, Atmos. Chem. Phys., p. 6003-6035).*

We have added the following description in the fifth paragraph of the introduction: "On the other hand, Stier et al. (2005) and Bauer et al. (2008) simulate externally mixed particles using modal aerosol models, where aerosol populations with different mixing states are represented by modes of different compositions (soluble/mixed or insoluble/not mixed). Although these models may be computationally cheap, they may not model accurately the dynamics of mixing."

•*2995-3: Section 2.1. (a) Somewhere in this section, explain how aerosol water is treated. E. g., are "m" (unsubscripted) and "d" the particle dry mass and diameter, or the wet ones? Is water calculated using an equilibrium approach? (b) Somewhere in this section, note that the composition sections/bins can be based on mass fractions of individual species, or mass fractions of groups of species, or a combination of the two.*

For question (a), water is treated separately from other species, the water content within each bin is computed using ISORROPIA before each loop of condensation/evaporation process. As specified on P.7942-L.16, d_p is the particle wet diameter while "m" stands for particle dry mass.

For question (b), the following sentence was added P.7943-L.19: "As $f_i = \frac{m_i}{m}$ is the mass fraction of species (or group of species) X_i, we may write:"

•*2995-8: Sections 2.1.4, 2.2, and 2.3 should be reorganized somewhat. These all discuss the numerical implementation of condensation/evaporation. I suggest putting them all into a Section 2.2 (Numerical implementation of condensation/evaporation). Begin this section with a brief discussion of how gas-particle mass transfer is first calculated in an aerosol chemistry module, then redistribution in size and composition space is calculated. Then Section 2.2.1 (Gas-particle mass transfer) would contain the current 2.1.4 and 2.2, and Section 2.2.2 (Redistribution) would contain the current 2.3.*

We reorganised the sections. Section 2.1 is now dedicated to the dynamic model of condensation/evaporation. This section presents the equations, their discretizations, the numerical implementation and the redistribution scheme. We have moved section 2.3 into section 2.1.5, so that all algorithms for solving dynamically condensation/evaporation are detailed in section 2.1. Section 2.2 is dedicated to the simplified algorithms that may be used instead of the dynamic approach to speed up the computation of condensation/evaporation (bulk equilibrium and hybrid approaches). Finally, section 2.3 explains the overall numerical structure of SCRAM,

including all the processes: not only condensation/evaporation but also coagulation and nucleation.

•*2995-15: P. 7953, L. 24-27. The changes to the HEMEM algorithm should be presented in more detail (perhaps in appendix), especially since Devilliers et al. (2013) do not clearly describe how the algorithm works when aerosol number and species masses are both predicted.*

Devilliers et al. (2013) studied the influence of redistribution on aerosol number and mass treated jointly, whereas previous papers had only studied the influence on either aerosol mass or number. The algorithm was not modified, except to allow the diameter of a section to grow larger than the upper bound diameter of the next section, as detailed in paragraph 2.1.5. For clarity, the following sentence was added to the paper: "In that case, the mean diameter of the section after condensation/evaporation is used to diagnose in which fixed-diameter sections the redistribution is performed."

•*2995-9: Section 2.3, near the end. Add a brief description of ordering details for the size and composition redistribution. E.g., is it sequential, with size redistribution done first, along the size axis for each of the composition bins, then composition redistribution done second, using the compositions after size redistribution? Note that with the moving diameter method, the redistribution could be done in a single step.*

The following paragraph is added at the end of the redistribution section:

"The composition redistribution is applied first, followed by the size redistribution for each of the composition sections."

•*2995-14: Section 2.4, title. Something like "Overall time integration and operator splitting in SCRAM" might be better.*

We have changed the section title as you suggested.

•*2995-16: Section 2.4, paragraph 2. Describe more clearly how nucleation is treated E.g., for each cond./evap./nucl. time sub-step, first calculate condensation/evaporation, then calculate nucleation, then do redistribution at the end of the multiple sub-steps.*

Section 2.3 now describes in greater detail of the time integration. The following sentence is added to the paper in Section 2.4, paragraph 2 before "Redistribution" on P.7955, L.4: "Condensation/evaporation/nucleation are solved simultaneously."

•*2996-2: This seems problematic if new particles could grow out of their initial size bin over multiple sub-steps.*

As we are using a lagrangian approach for solving condensation/evaporation, size bin boundaries are not fixed and they can grow freely with the particle within multiple sub-steps. However, the redistribution algorithm is systematically applied after condensation/evaporation, and it redistributes mass and number onto fixed size section boundaries.

•*2996-4: Also for nucleation, what is used for the H2SO4 vapour concentration? Is it a quasi steady state value that accounts for the simultaneous condensation loss*

and gas-phase chemistry production?

Gas-phase chemistry is not considered here in this 0D module. The H_2SO_4 vapour concentration available for condensation and nucleation is obtained from either emission or initial background concentration. Because condensation and nucleation are solved simultaneously, the same value of H_2SO_4 concentration is used for both processes.

•*Section 2.4, paragraph 3. Split this into separate paragraphs for the bulk equilibrium and hybrid approaches. In each paragraph, give full details of the ordering and sub-stepping of emissions, coagulation, cond/evap mass transfer, redistribution after cond/evap, and nucleation.*

We replaced section 2.4, paragraph 3. with the following two paragraphs: "When the bulk thermodynamic equilibrium approach is used to solve condensation/evaporation, coagulation then nucleation are solved after each emission time step. The resolution is done as previously explained, except that the dynamic condensation/evaporation solver is disabled: sub time steps are used to solve coagulation and nucleation during one emission time step. Condensation/evaporation is then solved using the bulk equilibrium approach and the redistribution process is applied after the bulk equilibrium algorithm."

"When the hybrid approach is used to solve condensation/evaporation, a time loop is added with a fixed time step of 600 s outside the emission time loop to compute bulk equilibrium condensation/evaporation for equilibrium sections. This additional time loop is designed to ensure that bulk equilibrium condensation/evaporation of equilibrium sections is not applied too often, so that the dynamic condensation/evaporation of dynamic sections has time to evolve. Redistribution is applied after the bulk equilibrium algorithm. Within this time loop, the aerosol dynamics is solved as previously explained using the dynamic condensation/evaporation algorithm for dynamic size sections: emissions are solved followed by coagulation and condensation/evaporation/nucleation. As in the fully dynamic approach, redistribution is applied after dynamic condensation/evaporation."

•*2996-11: P. 7955, L. 17-18. Provide a little more detail about the H2SO4 condensation. Do they specify a H2SO4 vapour source of about 0.46 $\mu m^3/cm^3/h$, or an initial concentration of 5.5 $\mu m^3/cm^3$, or something else?*

We are using a H_2SO_4 vapour source, so the P. 7955, L. 17-18. are updated to: "sulphuric acid vapour source of 0.46 $\mu m^3 cm^{-3}$ per hour"

•*2996-14: Figure 1 seems unnecessary. Just state in the text that for internal mixing, the initial particles are all 50% species 1 and 50% species 2; and for external mixing, half of the initial particles are 100% species 1 and the other half are 100% species 2.*

We removed figure 1 and replaced it with the suggested description.

•*Section 3, condensation plus coagulation test. It would be interesting to compare the performance with different numbers of composition bins. E.g., compare simulations with fewer bins (3-5 and 10) to a 100 bin "reference" simulation.*

As detailed in the major comment replies, following the reviewer's advice, the performance with different numbers of composition sections was added when testing

the condensation algorithm. We do not think that it would be useful to add a similar test for condensation plus coagulation.

•*Section 4.1, first paragraph. How are the gas concentrations treated? Do they just specify initial concentrations, or do they somehow include gas-chemistry production of condensible species such as H2SO4, HNO3, and semi-volatile organics.*

As previously explained, gas-phase-chemistry is not included in this 0-D model. Gas-phase concentrations are specified with initial concentrations and emissions (for H_2SO_4 and POA). They may also evolve because of condensation/evaporation.

•*2996-24: P. 7958, L. 24. Note in the text here that unmixed is used in an approximate sense, as all the composition bins allow some degree of mixing.*

We added this note in P.7958-L.24:

"Among them, there are 5 unmixed particles and 15 mixed particles. Here unmixed is used in an approximate sense: it means that the mass fraction of one chemical component is high (between 0.8 and 1), while the mass fraction of the other chemical components is low (between 0 and 0.2)."

•*2997-1: P. 7959, L. 13-16 and Figures 7-8. (a) There is considerable discussion (much of it on P. 7960) about the contributions of emissions vs. background particles to unmixed and mixed mass and number. This would be much clearer to readers if an additional plot were added to Figures 7 and 8 showing background (initial conditions) only. (b) The emissions contributions to BC and dust mass at large sizes will be clearer with this addition, but the CI of these emissions should be noted in the text, and also the actual BC and DU mass fractions of this CI for one or two of the larger sizes. (For some CI's, the mass fraction ranges for BC and dust are very wide.)*

We have added the distribution of initial conditions to figures 7 and 8. We also agree it is better to clarify the nature of emissions in the text, so the following sentences have been added at the end of the second paragraph of 4.2: "All emitted particles are unmixed: CI 1 (100% DU) into size section (4-6), CI 3 (100% BC) into size section (3-6). Emissions also involve POA and H_2SO_4 gas-phase emissions."

•*2997-9: I question this migration explanation. In Figure 8a, size bin 3 is mostly CI 3. Thus the coagulation of size bin 3 particles with size bin 4 particles would be dominated by [size 3, CI 3] particles with [size 4, CI 14] particles that could produce the [size 4, CI 15] particles.*

Thanks for the insightful argument, your explanation provides another possible path to the generation of CI 15 in size 4. Nevertheless, coagulation between [size 3, CI 15] particles themselves is also capable to produce [size 4, CI 15] particles. So we rewrote the analyse in P. 7959, L. 21.

"Also, due to coagulation, small particles migrated to higher sections. For example, Fig.8 shows the mixed particles CI 15 migrated from the third size section to the fourth size section, this might be a result of the coagulation between CI 3 particles in the third size section and the CI 14 in the fourth size section. Besides, coagulation between CI 5 particles in the third size section may also produce some part of CI 15 in the fourth size section."

•*2997-9: P. 7960, L. 3-4.Could be more specific here, and say that the [size 3,*

CI 5] particles come from condensation onto and transformation of [size 3, CI 3] particles

Thank you for your suggestion, we rewrote P. 7960, L. 3-4. :

"The condensation of organic matter on freshly emitted BC particles (CI 3) also occurs, as shown by the mixed BC and HBO particles (CI 5) which appear in the third and fourth size sections."

•*P. 7960, L. 8-10. State which pair of figures demonstrates this feature most clearly.*

We rewrote P. 7960, L. 8-10. :

"For example, as demonstrated by the difference between scenarios (C) and (D), newly mixed particles of CI 4 (between 20% and 80% of HBO) are formed by the coagulation of unmixed particles from CI 6 with others within the fourth and fifth size sections."

•*P. 7960, L. 13-17. This result (larger particles being better mixed) seems rather artificial, caused by (1) the assumption of all background particles being internally mixed and (2) the initial conditions dominating the large particles due to their low emissions and the short duration of the simulations. Large particles (especially coarse) are generally thought to be less internally mixed than fine particles. The authors should consider giving less emphasis to this result.*

Yes, indeed this result is rather artificial, and it is a consequence of the set up of the simulation. The purpose of this work is not to provide realistic based conclusions, which will be the purpose of future 3-D simulations. P. 7960, L. 13-17. is only trying to demonstrate how mixing occurs and to which extent. It is also an illustration of the basic informations that can be obtained from simulations. We rewrote this paragraph as follows:

"Table 2 shows the percentage of mixed particles for each scenario based on both particle number and mass concentrations. It seems that large particles are better mixed than small particles as the mixing percentages of mass are always higher than those of number. However, this phenomenon is specific to this case study; it is caused by the assumption of all initial particles being internally mixed and the initial conditions dominating for large particles due to their low emissions and the short duration of the simulations."

•*P. 7960, L. 19-21. This sentence seemed somewhat awkward to me. Maybe change to: "In scenario a, 42% (resp. 83%) of the particle number (resp. mass) originates from initial conditions and is mixed, while the remaining particles are due to emissions and are unmixed."*

We rewrote the sentence accordingly.

•*P. 7961, L. 14. The figure order (11 before 9 and 10) should be changed. If background (initial conditions) only plots are added to Figures 7 and 8 (see earlier comment), then the Figure 11 plots could also be put into Figure 7 and 8. This would make visual comparison of external vs. internal mixing results easier.*

We added both the initial conditions and internal mixing result distributions in figures 7 and 8 as suggested by the reviewer.

•*P. 7961, L. 21. Typo: TI6.*
We corrected TI6 into CI 6.

•*Section 4.3, paragraph 2. This discussion seems not of much value unless more quantitative details are provided. (See the last major comment above.) Consider size bin 4, which is CI 4 in internal mixing and CI 4 and 6 in external mixing. The actual mass fractions in the CI 6 could be quite close to those in the CI 4, in which case the internal/ external mixing differences would not be very important.*

More quantitative details about actual mass fraction of dominated species group were added in this paragraph. Indeed, the actual mass fraction in the CI 6 (81% HBO) is not so different from the one in the CI 4 (75.6%). However, it is interesting to keep the discussion in the paper, because it demonstrates the additional information provided by the external mixing results. Of course, we have to keep in mind that the difference between internally and externally mixed particles depends on the thresholds used to classify the particles.

•*Section 4.4. (a) The comparisons here should use the all processes simulations (with coagulation), since that is the most realistic, and turning off coagulation has a large impact (as seen in Fig. 7c vs. 7d, and 8c vs. 8d). (b) Since the focus of this paper is mixing state, the internally mixed results in this section should be removed, unless they are strongly needed to explain externally-mixed simulation differences between the dynamic, bulk equilibrium, and hybrid C/E methods.*

(a) Here, we focus on the impact of the different algorithms on mixing state, we want to study the impact of the simplified assumption of C/E computation on mixing state. Therefore, these studies are crucial. Adding coagulation would make the interpretation difficult and less accurate. These results are more process-oriented, rather than realistic. Realistic simulations will be performed with 3-D model coupled with SCRAM. (b) Comparisons to internally mixed results is also very important, because we want to compare the results obtained with different simplified assumptions (internally mixed assumption, bulk equilibrium C/E, hybrid C/E). For example, as stated in the paper "Although internal and external compositions are different with the dynamic approach, they are quite similar with the bulk equilibrium approach.". This is important to know, because it means that we should not bother with the externally mixed approach if we make the bulk equilibrium assumption.

•*P. 7963, L. 8-11. Point out that the speed of the hybrid C/E scheme is significantly degraded in the external mixing case. The number of size-composition bins increases by a factor of 20, but the hybrid C/E time increases by a factor of about 135. A brief explanation of why this happens would be of interest, although not necessary.*

For external mixing, the C/E hybrid scheme does not significantly improve the CPU time compared to the C/E dynamic scheme (whereas it does for internal mixing), probably because the redistribution after each time step between the different compositions leads to small time steps in the solver ROS2.

We added the following discussion into the end of 4.4 " This significant speed degradation of the hybrid C/E scheme in the external mixing case is probably a consequence of small time steps used in the ROS2 solver because of the redistribution

among the different composition sections performed after each time step. In other words, it takes CPU time to compute the dynamic distribution among the different composition sections."

•*Section 5. Add some discussion of computational costs.*

The following discussion about computational cost was added in section 5.

"Although the simulation of externally mixed particles increases the computational cost, SCRAM offers the possibility to investigate particle mixing state in a comprehensive manner. Besides, its mixing state representation is flexible enough to be modified by users. Better computational performance could be reached with fewer, yet appropriately specified species groups and more optimised composition discretisations. For example, about half of the 20 compositions designed in this work have really low mass concentrations (e.g. see Figures 7, 8, 9 and 10). Those compositions might be dynamically deactivated in the future version of SCRAM to lower computational cost by using an algorithm to skip empty sections during coagulation and C/E processing."

•*Table 1. Most of the numbers in the last column (DU) are incorrect. E.g., for composition bins 2-5, the DU fraction ranges are 0-80, 0-20, 0-80, 0-60, and 0-20%.*

We updated the table accordingly.

•*Figures 7-11. These should be improved in several ways. (a) The vertical bars should align better with the size section boundaries given on P. 7958, L. 9. (b) The density of the vertical or slanted lines in the vertical bars should match the line densities in the legends. (c) Some of the colors are difficult to distinguish. Since only about half of the 20 composition indices are visible in the plots, the CI's with negligible contributions to mass and number should be grouped into an "other" class (or possibly mixed-other and unmixed-other). E.g., any CI whose maximum mass and number concentrations are less than about 2% of 40 and 5e10, respectively, is not really visible in the plots and should go into the other class. This will reduce the number of colors needed, and colors that are more easily distinguished can be used. (This would be done on an all plots basis, not an individual plot basis.) Note that this would further highlight which CI's are important and which are not. (d) Each caption should list briefly the simulations shown in the figure: external/internal mixing, dynamic/bulk-equilibrium/ hybrid C/E solver, and which processes are active.*

We improved the figures based on the reviewer's suggestions.

References

[Kim and Seinfeld(1990)] Kim, Y. P. and Seinfeld, J. H.: Simulation of multicomponent aerosol condensation by the moving sectional method, Journal of Colloid and Interface Science, 135, 185–199, 1990.

2 Final response to Anonymous Referee 2

The authors thank the referee for providing a thorough review. We revised and clarified the paper as suggested. Each item starts with the reviewer's comment.

The manuscript by Zhu et al. presents the simulation results from a size - composition resolved aerosol box model SCRAM. After providing the detailed description regarding the model treatments, the authors conduct a couple of ideal case studies to demonstrate the ability of this box model in reproducing the reference results of Zhang et al. (1999). Finally additional case simulations are conducted by using a real case of model inputs from previous 3-D simulation results to show the impacts of different aerosol dynamic processes, mixing states (i.e., internal vs external mixing), and different assumptions for condensation/evaporation approaches on simulated aerosol mass and number distribution. This manuscript is generally well written with many interesting analyses. It's definitely of scientific interest to the atmospheric science community and I would recommend it to be accepted after a minor revision.

2.1 Specific Comments

• *One of the main reasons for majority of current 3-D atmospheric chemical transport or air quality models to use the assumption of internally-mixed aerosol treatment is the large computational cost, which could even make 3-D simulations impossible without sacrificing accuracy of aerosol representation (e.g., without reducing the number of aerosol species and size bins). The past studies have also found the overall aerosol mass and number concentrations could be very comparable for different aerosol size distributions between internal- and external-mixing. This point has also been verified in many occasions (in both text and figures) in Section 3 and 4 by this study. So I would really like to see some discussions in the conclusion section on how the current 3-D models can take advantage of and benefit from the treatment of external-mixing aerosols (such as the ability to predict the mixed states of aerosols) in SCRAM to compensate the loss of computational efficiency.*

We added the following discussion about mixing state and CPU time before the last paragraph of the conclusion section.

"Although the simulation of externally mixed particles increases the computational cost, SCRAM offers the possibility to investigate particle mixing state in a comprehensive manner. Besides, its mixing state representation is flexible enough to be modified by users. Better computational performance could be reached with fewer, yet appropriately specified species groups and more optimised composition discretisations. For example, about half of the 20 compositions designed in this work have really low mass concentrations (e.g. see Figures 4). Those compositions might be dynamically deactivated in the future version of SCRAM to lower computational cost by using an algorithm to skip empty sections during coagulation and C/E processing."

We also added discussions about the importance of the mixing state in the introduction:

"The mixing state assumption may strongly influence aerosol chemistry and the hygroscopic characteristics of particles. Particles from different origins may not be well mixed, and their chemical composition may vary with their origins, leading to variations in their hygroscopic characteristics. This chemical identity of particles is gradually lost as the degree of mixing increases (or completely lost under the internal mixing assumption). By influencing the hygroscopic characteristics of particles, the mixing state also influences the formation of secondary organic aerosols (SOA), because condensation/evaporation differs for species that are hydrophilic and/or hy-

drophobic (Couvidat et al., 2012). As the particle wet diameter is strongly related to the hygroscopic properties of particles, the mixing state also impacts particle wet diameters and the number of particles that become Cloud Condensation Nuclei (CCN), because the activation of particles into CCN is strongly related to particle wet diameter (Leck and Svensson, 2014). By influencing CCN, the mixing state also affects aerosol wet removal and thus the aerosol spatial/temporal distribution. Besides, the mixing state influences the particle optical properties, which depend on both the particle size distribution (wet diameters) and composition (different chemical species possess different absorption/scattering properties). Lesins et al. (2002) found that the percentage difference in the optical properties between an internal mixture and external mixture of black carbon and ammonium sulphate can be over 50% for wet aerosol. The mixing state may also influence radiative forcing, as shown by Jacobson (2001) who obtained different direct forcing results between external and internal mixing simulations of black carbon."

•*Page 7938, line 12: "thresholds of 12"; this is for primary aerosol only. There is another standard for secondary aerosol. May need to explicitly mention it here.*

We rewrote the sentence into:

"For example, regulatory concentration thresholds of 12 and 20 $\mu g\ m^{-3}$ have been set for $PM_{2.5}$ annual mass concentrations of primary aerosol in the United States and Europe, respectively."

•*Page 7940, lines 9-18: I don't suggest putting such detailed information in the introduction. If it's essential information that authors would like to deliver, they should move it into somewhere else such as the methodology section.*

We replaced the sentences by:

"Dergaoui et al. (2013) further expanded on these modelling approaches by discretising the mass fraction of any chemical species into sections, as well as the size distribution (see Section 2.1.3 for details)."

•*Page 7942, line 19: How do you select values of accommodation coefficient?*

The accommodation coefficient is set at 0.5, as now mentioned in the paper. There is a large uncertainty about the accommodation coefficient, which could vary between 0 and 1.

•*Page 7943, line 6: which version of ISORROPIA here?*

We are using ISORROPIA v1.7 here, as now stated.

•*Page 7956, lines 11-12: I wouldn't say it's a perfect match since there is a little difference for the peak values of number distribution.*

We replaced "perfect" by "good".

•*Page 7957, Section 4: It seems the SOA formation is not included in SCRAM and it has to rely on the other SOA modules if incorporated into 3-D models? It should be indicated in the manuscript.*

In SCRAM, SOA originate either from initial conditions or they are emitted as semi-volatile organic compounds during the simulation. They are not oxidized, as the gas chemistry is not included in SCRAM. Yes, the gas chemistry will be solved

in 3-D simulation with other modules. We updated our manuscript to specify this at the end of the second paragraph of 4.1:

"Besides, gas chemistry (such as SOA formation) is not included in SCRAM, and is expected to be solved separately using a gas chemistry scheme. In the simulations of this paper, organics originate either from initial conditions or they are emitted as semi-volatile organic compounds during the simulation. They do partition between the gas and the aerosol phases by condensation/evaporation."

•*Page 7957, line 25: deposition is also ignored here and should be mentioned.*

We updated the description into:

"As our simulations are 0D, the transport of gases and particles and the deposition processes are not taken into account."

•*Page 7958, line 8: why choose 7 sections? Many existing aerosol modules typically use 4/8/12-bin structures.*

We chose 7 sections here because we obtained the initial condition data from existing and published 3D simulation results (of SIREAM) with 7 size sections.

•*Page 7958, line 12: When you grouped them, does the model still be able to track the concentrations of individual species (this is very important!). How do you treat individual species within each group for mass fraction sections? Such information is expected here.*

Yes the model can still track the concentration of individual species. The model memorizes the relationship between each species index and group index, and stores the mass concentration separately for each species within each size-composition bins. The total mass concentration of each group is computed from the mass concentration of each species based on the species-group relations, allowing the computation of the mass fraction of each group. We added this explanation at the end of this paragraph: Page 7958, line 27.

•*Page 7959, line 3: change all the scenario names to upper cases (e.g., a to A and b to B).*

We updated the scenario names accordingly.

•*Page 7960, lines 13-15: this seems to be conflicted with our general understanding that fine-mode particles are much easier internally-mixed than coarse-mode particles.*

It is caused by the internal mixing assumption we made for the initial particles. The following sentences were added to explain this:

" It seems that large particles are better mixed than small particles as the mixing percentages of mass are always higher than those of number. However this phenomenon is specific to this case study; it is caused by the assumption of all initial particles being internally mixed and the initial conditions dominating for large particles due to their low emissions and the short duration of the simulations."

•*Page 7961, line 14: I didn't see that Figures 9 and 10 were mentioned before this. Please don't jump the figure numbers.*

We rearranged the figure orders.

•*Page 7963, line 8: The information provided in this table indicates that the CUP time required by the external-mixing for the current box model could significantly slow down the simulation. I would expect some discussion on how this box model could be incorporate in a feasible way into 3-D models without reducing the number of size bins and mass fraction sections (which are keys for accurate simulations of externally-mixed aerosol processes). Are there any rooms for authors to optimize the code to further reduce he computational time, because I am not sure if the current performance in terms of CPU time is acceptable for the 3-D implementation?*

We are currently working on the 3D implementation, which will be presented in another paper. We just managed to successfully run 3-D simulations with SCRAM with a reasonable CPU time (about 8 times slower than the internal mixing case for a dynamic C/E + coagulation simulation) without compromising any size and mass fraction sections. Some discussion about computation costs and optimization has been added in the conclusion as mentioned earlier in the reply.

•*Page 7963, line 11: C/E; this acronym should be defined much earlier in Section 4.2.*

We moved up this definition to the first paragraph of Section 4.2.

•*Page 7963, lines 24-25: I was looking for this information when I read Section 2. I would suggest adding this information where it is appropriate.*

Thank you for your suggestion, we have added this information at the beginning of Section 2.1.3:

"As SCRAM is a size-composition resolved model, both particle size and composition are discretised into sections, while the numbers and bounds of both size and composition sections can be customised by the user."

•*Page 7964, lines 23-24: Again I am really not sure how feasible it could be to incorporate the current box model into 3-D considering the huge increase of computation cost between the internal- and external-mixed results.*

see reply above.

•*Figure 2: Can you replace the lines for reference and internal cases with markers?*

Thank you for your advice, we have replaced the lines for reference and internal cases with markers as you suggested.

•*Figure 6: Is it UTC or local time?*

It is UTC, we updated figure 6 to specify that.

Technical notes:

Thank you for your detailed technical notes, all of them have been taken into account accordingly.

3 List of all relevant changes

All the line numbers provide in the following list correspond to the line number marked on the difference marked-up manuscript version include at the end of the document.

1. Line 6: Abstract: replaced the final sentence by *"The degree of mixing of particles is investigated in a box model simulation using data representative of air pollution in Greater Paris. The relative influence on the mixing state of the different aerosol processes (condensation/evaporation, coagulation) and of the algorithm used to model condensation/evaporation (bulk equilibrium, dynamic) is studied."*.

2. Line 20: At the beginning of second paragraph of Introduction, replaced the upper case "Chemical" by lower case "chemical".

3. Line 37: Completely rewrite the fourth paragraph of Introduction to emphasize the importance of particle mixing state to aerosol properties.

4. Line 66: Added two new references about modal aerosol models at the middle of fifth paragraph of introduction with a brief discussion.

5. Line 76: Change "composition" to plural form "compositions".

6. Line 78: Removed the detailed description of size-composition discretisation from the fifth paragraph and replaced by "*see Section 2.1.3 for details*".

7. Line 90: Correct "expends" to "expands".

8. Line 120: Add an explanation to clarify the relationship between the lagrangian approach and redistribution method.

9. Line 154: Explained that X_i can be the mass fraction of either species or group of species.

10. Line 164: At the beginning of section 2.1.3, specified that "*while the numbers and bounds of both size and composition sections can be customised by the user.*".

11. Line 168: Complement "species" with "species or species groups" .

12. Line 183: Section 2.1.3, removed the derivations of equation (10) and (9) (namely from equation (9-16) in original manuscript) and replaced them on Appendix B.

13. Line 215: Rearrange section 2.2 (Size and composition redistribution) into section 2.1.5..

14. Line 259 and Line 260: Add "the" before "highest".

15. Line 263: Add following explanation for the modification of Deilliers' method "*In that case, the mean diameter of the section after condensation/evaporation is used to diagnose in which fixed-diameter sections the redistribution is performed.*".

16. Line 271: Specified the redistribution method for composition redistribution with "*i.e., moving mass fraction*".

17. Line 274: Replaced "which" by "that".

18. Line 278: Add an explanation of redistribution orders " *The composition redistribution is applied first, followed by the size redistribution for each of the composition sections.*"

19. Line 281: Section 2.2 is remain the same.

20. Line 309: The original Section 2.4 (Time resolution of SCRAM) is now become Section 2.3 (Overall time integration and operator splitting in SCRAM)

21. Line 322: Add a sentence "*Then, condensation/evaporation/nucleation are solved simultaneously.*"

22. Line 328: Split the original paragraph into two, explained the time integration structure of bulk equilibrium and hybrid method separately in each new paragraph.

23. Line 352: Specified the sulphuric acid vapour source.

24. Line 354: Changed "ATM" into "atm"

25. Line 359 and Line 364: Removed the original Figure 1 (Line 364) and explained the initial composition distribution by text (Line 359).

26. Line 371, Line 373 and Line 387: replace "perfect match" with "good match".

27. Line 372: Replace "a 100%" with "an almost 100%".

28. Line 374: A new discussion is added to investigate the influence of the composition resolution on simulation results. The newly added figure 2 corresponds to this part of discussion.

29. Line 411: Change "at" to "on".

30. Line 413: Add "N" and "E" to specified the coordinated of simulation location.

31. Line 419: Specified that the deposition processes are not taken into account.

32. Line 425: Additional explanation is provide here to clarify that gas-phase chemistry is not included in SCRAM and how the gas concentrations are generated and treated.

33. Line 434: Details about the how species group are chosen is added here.

34. Line 451: New discussion is provide here to specify the notion of unmixed particle within this paper.

35. Line 454: Add an explanation why the dust is chosen as the default group which is not treated explicitly and possible alternatives exist to change the default group or even have all groups be treated explicitly.

36. Line 463: A new paragraph is added here to explain how the relations between species and each group is treated within SCRAM as well as the storage of mass concentration.

37. Line 468: All letters correspond to each simulation scenario (a, b, c, d, e, f) is changed into capital letter (A, B, C, D, E, F) here after.

38. Line 470: Moved up the definition of abbreviation of "condensation/evaporation (C/E)", and replace condensation/evaporation by C/E here after.

39. Line 475: Specified the add of the initial size-composition distribution in sub-figure (e).

40. Line 477: Specified the that all CI with tiny concentrations are regrouped into mixed-other or unmixed-other group in these new size-composition distribution plots.

41. Line 480: Provide some details about emissions.

42. Line 488: Specified "small particles".

43. Line 489: Rewrite the sentence.

44. Line 490: Addition possibility is provide thanks to Referee 1 to explain the migration of CI 15.

45. Line 496: Add the explanation about how the exact mass fraction will be showed in this paper. And exact mass fraction is added to each dominate group of different composition mentioned in this paper here after.

46. Line 501: Change "particle" to "particles".

47. Line 504: Rewrite the sentence to provide better description.

48. Line 509: Offered additional description for better explanation.

49. Line 513: This paragraph is reorganised to improve the discussion about the special mixing result between different scenarios.

50. Line 520: Reformulate the sentence.

51. Line 543: Updated the figure label based on new figures.

52. Line 550: Correct "TI" by "CI".

53. Line 571 and 572: Delete repeated "Figures".

54. Line 578: Correct wrong number.

55. Line 592: Added "the" before lowest.

56. Line 598: Deleted "time" and provide possible explanation for the significant degrade of hybrid method efficiency.

57. Line 616: Replace "emission typical" by "typical emission".

58. Line 620: Replace "detail" by "details".

59. Line 632: Replace "similarly to" by "as observed with".

60. Line 633: Additional paragraph is added here to discuss possible optimisations for improving the computation efficiency of SCRAM.

61. Line 641: Add "optimisation and" in the first sentence.

62. Page 32: Original Figure 1 was removed.

63. Page 32-33: Makers has been added onto Figure 1 and 3 to offer a clearer presentation.

64. Page 32: Figure 2 is newly added to present the influence of different compositions resolution to mixing results.

65. Page 35-38: Both the bar width and color bar are improved for figure 7-10, in order to offer a better presentation. Additional information was also added in the caption to specify which scenario is present in the figure.

66. Page 35-36: Both initial condition and internal mixing result are now added to figure 7 and 8. While the original Figure 11 was deleted.

67. Page 39: The mass fraction ranges of last group "DU" were updated in table 1.

4 Marked-up manuscript version:

Manuscript prepared for Geosci. Model Dev.
with version 2014/07/29 7.12 Copernicus papers of the LaTeX class copernicus.cls.
Date: 10 February 2015

A size-composition resolved aerosol model for simulating the dynamics of externally mixed particles: SCRAM (v 1.0)

Shupeng Zhu[1], Karine N. Sartelet[1], and Christian Seigneur[1]

[1]CEREA, joint laboratory Ecole des Ponts ParisTech - EDF R&D, Université Paris-Est, 77455 Champs-sur-Marne, France.

Correspondence to: S. Zhu
(zhus@cerea.enpc.fr)

Abstract. A Size-Composition Resolved Aerosol Model (SCRAM) for simulating the dynamics of externally-mixed atmospheric particles is presented. This new model classifies aerosols by both composition and size, based on a comprehensive combination of all chemical species and their mass-fraction sections. All three main processes involved in aerosol dynamics (coagulation, condensation/evaporation and nucleation) are included. The model is first validated by comparison with a reference solution and with results of simulations using internally-mixed particles. The ~~importance of representing the mixing state when modelling atmospheric aerosol concentrations~~ degree of mixing of particles is investigated in a box model simulation using data representative of air pollution in Greater Paris. The relative influence on the mixing state of the different aerosol processes (condensation / evaporation, coagulation) and of the algorithm used to model condensation/evaporation (bulk equilibrium, dynamic) is studied.

1 Introduction

Increasing attention is being paid to atmospheric particulate matter (PM), which is a major contributor to air pollution issues ranging from adverse health effects to visibility impairment (EPA, 2009; Pascal et al., 2013). Concentrations of $PM_{2.5}$ and PM_{10} are regulated in many countries, especially in North America and Europe. For example, regulatory concentration thresholds of 12 and 20 $\mu g\ m^{-3}$ have been set for $PM_{2.5}$ annual mass concentrations in the United States and Europe, respectively. Furthermore, particles influence the Earth's energy balance and global climate change (Myhre et al., 2013).

Three-dimensional ~~Chemical transport~~ chemical-transport models (CTM) are often used to study and forecast the formation and distribution of PM. The size distribution of particles is often discretised into sections (e.g., Gelbard and Seinfeld, 1980; Zhang et al., 2004; Sartelet et al., 2007) or approximated by log-normal modes (e.g., Whitby and McMurry, 1997; Binkowski and Roselle, 2003). Moreover, CTM usually assume that particles are internally-mixed, i.e. each size section or log-normal mode has the same chemical composition, which may vary in space and time.

The internal-mixing assumption implies that particles of a same diameter (or in the same size section or log-normal mode) but originating from different sources have undergone sufficient mixing to achieve a common chemical composition for a given model grid cell and time. Although this assumption may be realistic far from emission sources, it may not be valid close to emission sources where the composition of new emitted particles can be very different from either background particles or particles from other sources. Usually, internally- and externally-mixed particles are not differentiated in most measurements, which may be size-resolved (e.g., cascade impactors) but not particle specific (McMurry, 2000). The use of mass spectrometers for individual particle analysis has shed valuable information on the chemical composition of individual particles. Consequently, there is a growing body of observations indicating that particles are mostly externally mixed (e.g., Hughes et al., 2000; Mallet et al., 2004; Healy et al., 2012; Deboudt et al., 2010).

The mixing state assumption may strongly influence aerosol chemistry and ~~hygroscopic characteristics , influencing in turn particle diameters, optical properties,~~ the hygroscopic characteristics of particles. Particles from different origins may not be well mixed, and their chemical composition may vary with their origins, leading to variations in their hygroscopic characteristics. This chemical identity of particles is gradually lost as the degree of mixing increases (or completely lost under the internal mixing assumption). By influencing the hygroscopic characteristics of particles, the mixing state also influences the formation of secondary organic aerosols (SOA), because condensation/evaporation differs for species that are hydrophilic and/or hydrophobic (Couvidat et al., 2012) . As the particle wet diameter is strongly related to the hygroscopic properties of particles, the mixing state also impacts particle wet diameters and ~~radiative forcing (Lesins et al., 2002; Jacobson, 2001) , and~~ the number of particles that ~~may~~ become cloud condensation nuclei (CCN), because the activation of particles ~~depends on their size and composition (Leck and Svensson, 2014) .~~ into CCN is strongly related to the particle wet diameter (Leck and Svensson, 2014) . By influencing CCN, the mixing state also affects aerosol wet removal and thus the aerosol spatial/temporal distribution. Besides, the mixing state influences the particle optical properties, which depend on both the particle size distribution (wet diameters) and composition (different chemical species possess different absorption / scattering properties). Lesins et al. (2002) found that the percentage difference in the optical properties between an internal mixture and external mixture of black carbon and ammonium sulphate can be over 50% for wet aerosols. The mixing state may also influence ~~the formation of secondary organic aerosols (SOA), by influencing the hydrophilic and /or organic absorbing properties of~~

particlesradiative forcing, as shown by Jacobson (2001) who obtained different direct forcing results between external and internal mixing simulations of black carbon.

Although CTM usually assume that particles are internally-mixed, several models have been developed during the last sesquidecade to represent the external mixture of particles. A source-oriented model was developed by Kleeman et al. (1997) and Kleeman and Cass (2001) for regional modelling. In these models, each source is associated with a specific aerosol population, which may evolve in terms of size distribution and chemical composition, but does not mix with the other sources (i.ee., particle coagulation is neglected). Riemer et al. (2009) modelled externally-mixed particles using a stochastic approach. However, such an approach is computationally expensive when the number of particles particle species is high. On the other hand, Stier et al. (2005) and Bauer et al. (2008) simulate externally mixed particles using modal aerosol models, where aerosol populations with different mixing states are represented by modes of different compositions (soluble / mixed or insoluble/not mixed). Although these models may be computationally efficient, they may not model accurately the dynamics of mixing. To represent externally-mixed particles independently of their sources and number concentrations, Jacobson et al. (1994) and Lu and Bowman (2010) considered particles that can be either internally- or externally-mixed (i.e., composed of a pure chemical species). Lu and Bowman (2010) used a threshold mass fraction to define whether the species is of significant concentration. Jacobson (2002) expanded on Jacobson et al. (1994) by allowing particles to have different mass fractions. Similarly, Oshima et al. (2009) discretised the fraction of black carbon in the total particle mass into sections of different chemical compositioncompositions. Dergaoui et al. (2013) further expanded on these modelling approaches by discretising the mass fraction of any chemical species into sections, as well as the size distribution . For each size section, the mass fraction of each species is discretised into sections $F_h{}_-^+ = [F_h{}^-, F_h{}^+]$ (h varies from 1 to the number of mass fraction sections n_f with $F_1{}^- = 0$, $F_{n_f}{}^- = 1$ and $F_h{}^- = F_{h-1}{}^+$]), leading to a variety of possible particle compositions. Assuming that it is possible to have up to c chemical species in particles, let us denote f_i the mass fraction of species X_i ($1 \leq i \leq c$). Each particle is associated with a mass fraction vector $=(f_1, f_2, \cdots, f_{(c-1)})$, which defines the particle composition/ $=(F_{g_1}{}_-^+, F_{g_2}{}_-^+, \cdots, F_{g_{(c-1)}}{}_-^+)$ with $f_i \in F_{g_i}{}_-^+$. For a particle composition to be valid, $\sum_{i=1}^{(c-1)} F_{g_i}{}^- \leqslant 1$ must be satisfied. Note that f_c is not specified because it is constrained by mass conservation ($f_c = 1 - \sum_{i=1}^{(c-1)} f_i$). see Section 2.1.3 for details). Based on this discretisation, Dergaoui et al. (2013) derived the equation for coagulation and validated their model by comparing the results obtained for internal and external mixing, as well as by comparing both approaches against an exact solution. However, processes such as condensation/evaporation and nucleation were not modelled.

This work presents a new Size-composition Resolved Aerosol Model (SCRAM), which expends expands on the model of Dergaoui et al. (2013) by including condensation/evaporation and nucleation processes. Section 2 describes the model. Equations for the dynamic evolution of particles by condensation/evaporation are derived. A thermodynamic equilibrium method may be used in

SCRAM to compute the evolution of the particle chemical composition by condensation/evaporation. Redistribution algorithms, which allow section bounds not to vary, are also presented for future 3D applications. Model validation is presented in Section 3 by comparing the changes in the particle size distribution due to condensational growth for both externally- and internally-mixed particles. Section 4 presents an application of the model with realistic concentrations over Greater Paris.

2 Model Description

This section presents the aerosol general dynamic equations and the structure of the model. First, the formulation of the dynamic evolution of the aerosol size distribution and chemical composition by condensation-evaporation is introduced. Since it is necessary in 3D CTM to maintain fixed size and composition section bounds, we present algorithms to redistribute particle mass and number according to fixed section bounds. For computational efficiency, a bulk equilibrium method, which assumes an instantaneous equilibrium between the gas and particle phases, is introduced. Finally, the overall structure of the model is described. In particular, the treatment of the different mixing processes to ensure the numerical stability of the model is discussed.

Particle dynamics is mostly governed by three processes: coagulation, condensation/evaporation, and nucleation. Nucleation refers to the formation of ultra fine particles from gaseous molecules. SCRAM uses the parametrisation of Vehkamäki et al. (2002) for the homogeneous binary nucleation of sulphate and water. It was adopted from the existing SIREAM code (Debry et al., 2007). It may be replaced by a better parametrisation in future versions, because it may lead to unrealistic results under some extreme conditions (Zhang et al., 2010). For coagulation, SCRAM uses the code of Dergaoui et al. (2013) to simulate the collisions of particles caused by Brownian motion. Condensation/evaporation describe the mass transfer process between the gas and the particle phases. It is essential to include condensation/evaporation, because this process not only largely influences the size distribution of aerosols, but may also change the composition of particles significantly.

2.1 Condensation-Evaporation Algorithm

The focus of the following subsections is the formulation and implementation of the condensation/evaporation process. A lagrangian approach is used to solve the equations of change for the mass and number concentrations, which are redistributed onto fixed sections through a redistribution algorithm (moving diameter, Jacobson (1997)). Equations are derived to describe the change with time of the mass concentrations of chemical species in terms of particle compositions.

2.1.1 Dynamic equation for condensation/evaporation

Let us denote m_i the mass concentration of species X_i ($1 \leq i \leq c$) in a particle and $\boldsymbol{x}$ the vector representing the mass composition of the particle $\boldsymbol{x} = (m_1, m_2, \cdots, m_c)$. Following Riemer et al.

(2009), the change with time of the number concentration $n(\boldsymbol{x},t)$ (m^{-3} $\mu\mathrm{g}^{-1}$) of multi-species particles by condensation/evaporation can be represented by the following equation:

$$\frac{\partial n}{\partial t} = -\sum_{i=1}^{c} \frac{\partial (I_i n)}{\partial m_i} \tag{1}$$

where I_i ($\mu\mathrm{g\ s}^{-1}$) is the mass transfer rate between the gas and particle phases for species X_i. It may be written as follows:

$$I_i = \frac{\partial m_i}{\partial t} = 2\pi\ D_i^g\ d_p\ f(K_n,\alpha_i)(c_i^g(t) - K_e(d_p)\ c_i^{eq}(\boldsymbol{x},t)) \tag{2}$$

where D_i^g is the molecular diffusivity of condensing/evaporating species in the air, and d_p and c_i^g are the particle wet diameter and the gas phase concentration of species X_i, respectively. Non-continuous effects are described by $f(K_n,\alpha_i)$ (Dahneke, 1983) which depends on the Knudsen number, $K_n = \dfrac{2\lambda}{d_p}$ (with λ the air mean free path), and on the accommodation coefficient ~~α_i~~ $\alpha_i = 0.5$:

$$f(K_n,\alpha_i) = \frac{1+K_n}{1+2K_n(1+K_n)/\alpha_i} \tag{3}$$

$K_e(d_p)$ represents the Kelvin effect (for ultra fine particles, the curvature tends to inhibit condensation):

$$K_e(d_p) = exp\left(\frac{4\ \sigma\ v_p}{R\ T\ d_p}\right) \tag{4}$$

with R the ideal gas constant, σ the particle surface tension and v_p the particle molar volume. The local equilibrium gas concentration c_i^{eq} is computed using the reverse mode of the thermodynamic model ISORROPIA V1.7 (Nenes et al., 1998) for inorganic compounds. In the current version of SCRAM, organic compounds are assumed to be at thermodynamic equilibrium with the gas phase and condensation/evaporation is computed as described in Section 2.2.

2.1.2 Dynamic equation as a function of mass fractions

Following the composition discretisation method of Dergaoui et al. (2013) (detailed in Section 2.1.3), each particle is represented by a vector $\boldsymbol{p}$=($\boldsymbol{f}$,m), which contains the mass fraction vector $\boldsymbol{f}$=($f_1, f_2, \cdots, f_{(c-1)}$) of the first $(c-1)$ species and the total mass $m = \sum_{i=1}^{c} m_i$.

In Equation (1), the chemical composition of particles is described by the vector $\boldsymbol{x}$, which contains the mass concentration of each species. After the change of variable through a $[c \times c]$ Jacobian matrix from $n(\boldsymbol{x},t)$ to $\bar{n}(\boldsymbol{p},t)$ (see Appendix A for detail), Equation (1) becomes:

$$\frac{\partial \bar{n}}{\partial t} = -\sum_{i=1}^{(c-1)} \frac{\partial (H_i \bar{n})}{\partial f_i} - \frac{\partial (I_0 \bar{n})}{\partial m} \tag{5}$$

with $I_0 = \sum_{i=1}^{c} I_i$, $H_i = \dfrac{\partial f_i}{\partial t}$. As $f_i = \dfrac{m_i}{m}$ is the mass fraction of species (or group of species) X_i, we may write:

$$H_i = \frac{1}{m}\frac{\partial m_i}{\partial t} - \frac{m_i}{m^2}\frac{\partial m}{\partial t} = \frac{I_i - f_i I_0}{m} \tag{6}$$

The change with time of $q_i = n\ m_i$, the mass concentration of species X_i, can be expressed as follows:

$$\frac{\partial q_i}{\partial t} = \frac{\partial n}{\partial t} m_i + \frac{\partial m_i}{\partial t} n \tag{7}$$

After the change of variables from $q_i(\boldsymbol{x},t)$ to $\bar{q}_i(\boldsymbol{p},t)$ (see Appendix A), Equation (7) becomes:

$$\frac{\partial \bar{q}_i}{\partial t} = -m\ f_i \frac{\partial \bar{n}}{\partial t} + \bar{n}\ I_i \tag{8}$$

2.1.3 Discretisation

As SCRAM is a size-composition resolved model, both particle size and composition are discretised into sections, while the numbers and bounds of both size and composition sections can be customised by the user. The particle mass distribution $Q[m_{min}, m_{max}]$ is first divided into N_b size sections $[m_k^-, m_k^+]$ ($k = 1, ..., N_b$ and $m_{k-1}^+ = m_k^-$), defined by discretising particle diameters $[d_{min}, d_{max}]$ with d_{min} and d_{max}, the lower and upper particle diameters, respectively, and $m_k = \frac{\pi\ \rho\ d_k^3}{6}$. For each of the first $(c-1)$ species or species groups, the mass fraction is discretised into N_f fraction ranges. The h^{th} fraction range is represented by the range $F_h{}_-^+ = [f_h^-, f_h^+]$ where $f_{h-1}^+ = f_h^-$, $f_{min} = 0$ and $f_{max} = 1$. Within each size section k, particles are categorised into N_p composition sections, which are defined by the valid combinations of the fraction ranges of the $(c-1)$ species. The g^{th} composition section can be represented by $\boldsymbol{P_g}$=$(F_{g1}{}_-^+, F_{g2}{}_-^+, \cdots, F_{gc-1}{}_-^+)$. Given the mass fraction discretisation, those composition sections are automatically generated by an iteration on all possible combinations ($N_f{}^{(c-1)}$) of the $(c-1)$ species and N_f fraction ranges. Only the composition sections that satisfy $\sum_{i=1}^{(c-1)} F_{gi}{}^- \leqslant 1$ are kept.

The particle mass distribution is discretised into $(N_b \times N_p)$ sections. Each section j ($j = 1, ..., N_b \times N_c$) corresponds to a size section k ($k = 1, ..., N_b$) and to a composition section $g = (g_1, ..., g_{(c-1)})$ with $g = 1, ..., N_p$, $g_h = 1, ..., N_f$ with $h = 1, ..., (c-1)$. The total concentration Q_i^j of species i in the j^{th} section can be calculated as follows:

$$Q_i^j = \int_{m_k^-}^{m_k^+} \int_{f_{g1}^-}^{f_{g1}^+} ... \int_{f_{g(c-1)}^-}^{f_{g(c-1)}^+} \bar{q}_i(m, f_{g_1}, ..., f_{g_{(c-1)}}) dm df_{g_1} ... df_{g_{(c-1)}} \tag{9}$$

Similarly, the number concentration N^j of the j^{th} section may be written as follows:

$$N^j = \int_{m_k^-}^{m_k^+} \int_{f_{g1}^-}^{f_{g1}^+} ... \int_{f_{g(c-1)}^-}^{f_{g(c-1)}^+} \bar{n}(m, f_{g_1}, ..., f_{g_{(c-1)}}) dm df_{g_1} ... df_{g_{(c-1)}} \tag{10}$$

~~The~~ After a series of derivations (see Appendix B for details), we obtain the time derivation of Equation (10)~~leads to:~~

$$\frac{\partial N^j}{\partial t} = \overbrace{\int_{m_k^-}^{m_k^+}\int_{f_{g1}^-}^{f_{g1}^+}\dots\int_{f_{g(c-1)}^-}^{f_{g(c-1)}^+}\frac{\partial \bar{n}}{\partial t}dmdf_{g_1},...,df_{g_{(c-1)}}}^{A}$$

$$\overbrace{+\frac{dm_k^+}{dt}\int_{f_{g1}^-}^{f_{g1}^+}\dots\int_{f_{g(c-1)}^-}^{f_{g(c-1)}^+}\bar{n}(m_k^+,f_{g_1},...,f_{g_{(c-1)}})df_{g_1},...,df_{g_{(c-1)}} - \frac{dm_k^-}{dt}\int_{f_{g1}^-}^{f_{g1}^+}\dots\int_{f_{g(c-1)}^-}^{f_{g(c-1)}^+}\bar{n}(m_k^-,f_{g_1},...,f_{g_{(c-1)}})df_{g_1},...,df_{g_{(c-1)}}}^{B}$$

$$+\sum_{i=1}^{(c-1)}\left[\frac{df_{g_i}^+}{dt}\int_{m_k^-}^{m_k^+}\int_{f_{g1}^-}^{f_{g1}^+}\dots\int_{f_{g_{i-1}}^-}^{f_{g_{i-1}}^+}\int_{f_{g_{i+1}}^-}^{f_{g_{i+1}}^+}\dots\int_{f_{g(c-1)}^-}^{f_{g(c-1)}^+}\bar{n}(m,f_{g_1},...,f_{g_{i-1}},f_{g_i}^+,f_{g_{i+1}},...,f_{g_{(c-1)}})dmdf_{g_1}...df_{g_{i-1}}df_{g_{i+1}}...df_{g_{(c-1)}}\right.$$

$$\left.-\frac{df_{g_i}^-}{dt}\int_{m_k^-}^{m_k^+}\int_{f_{g1}^-}^{f_{g1}^+}\dots\int_{f_{g_{i-1}}^-}^{f_{g_{i-1}}^+}\int_{f_{g_{i+1}}^-}^{f_{g_{i+1}}^+}\dots\int_{f_{g(c-1)}^-}^{f_{g(c-1)}^+}\bar{n}(m,f_{g_1},...,f_{g_{i-1}},f_{g_i}^-,f_{g_{i+1}},...,f_{g_{(c-1)}})dmdf_{g_1}...df_{g_{i-1}}df_{g_{i+1}}...df_{g_{(c-1)}}\right]$$

~~Replacing $\frac{\partial \bar{n}}{\partial t}(m,f_{g_1},...,f_{g_{(c-1)}})$ by Equation (5), we have~~

$$A = \int_{m_k^-}^{m_k^+}\int_{f_{g1}^-}^{f_{g1}^+}\dots\int_{f_{g(c-1)}^-}^{f_{g(c-1)}^+}\left[-\frac{\partial(I_0 n)}{\partial m} - \sum_{x=1}^{(c-1)}\frac{\partial(H_{g_x}n)}{\partial f_{g_x}}\right]dmdf_{g_1}...df_{g_{(c-1)}}$$

~~and using $I_0 = \frac{dm}{dt}$, $H_{g_i} = \frac{df_{g_i}}{dt}$ and $\frac{\partial f_{g_i}}{\partial f_{g_l}} = 0$ when $i \neq l$~~

$$A = -\left\{\frac{dm_k^+}{dt}\int_{f_{g1}^-}^{f_{g1}^+}\dots\int_{f_{g(c-1)}^-}^{f_{g(c-1)}^+}\bar{n}(m_k^+,f_{g_1},...,f_{g_{(c-1)}})dmdf_{g_1}...df_{g_{(c-1)}} - \frac{dm_k^-}{dt}\int_{f_{g1}^-}^{f_{g1}^+}\dots\int_{f_{g(c-1)}^-}^{f_{g(c-1)}^+}\bar{n}(m_k^-,f_{g_1},...,f_{g_{(c-1)}})dmdf_{g_1}...df_{g_{(c-1)}}\right.$$

$$+\sum_{i=1}^{(c-1)}\left[\frac{df_{g_i}^+}{dt}\int_{m_k^-}^{m_k^+}\int_{f_{g1}^-}^{f_{g1}^+}\dots\int_{f_{g_{i-1}}^-}^{f_{g_{i-1}}^+}\int_{f_{g_{i+1}}^-}^{f_{g_{i+1}}^+}\dots\int_{f_{g(c-1)}^-}^{f_{g(c-1)}^+}\bar{n}(m,f_{g_1},...,f_{g_{i-1}},f_{g_i}^+,f_{g_{i+1}},...,f_{g_{(c-1)}})dmdf_{g_1}...df_{g_{i-1}}df_{g_{i+1}}...df_{g_{(c-1)}}\right.$$

$$\left.\left.-\frac{df_{g_i}^-}{dt}\int_{m_k^-}^{m_k^+}\int_{f_{g1}^-}^{f_{g1}^+}\dots\int_{f_{g_{i-1}}^-}^{f_{g_{i-1}}^+}\int_{f_{g_{i+1}}^-}^{f_{g_{i+1}}^+}\dots\int_{f_{g(c-1)}^-}^{f_{g(c-1)}^+}\bar{n}(m,f_{g_1},...,f_{g_{i-1}},f_{g_i}^-,f_{g_{i+1}},...,f_{g_{(c-1)}})dmdf_{g_1}...df_{g_{i-1}}df_{g_{i+1}}...df_{g_{(c-1)}}\right]\right\}$$

~~So $A = -B$, thus~~

$$\frac{\partial N^j}{\partial t} = (A+B) = 0$$

~~which is expected since condensation/evaporation does not affect the total number of particles. :~~

~~Similarly, an equation of change can be derived for Q_i^j. In order to simplify the writing of the equations, the following abbreviations are introduced:~~

$$f_{g_1^{(c-1)}} = f_{g_1}, ..., f_{g_{(c-1)}}$$

$$f_{g_1^{(c-1)} \setminus i} = f_{g_1}, ..., f_{g_{i-1}}, f_{g_{i+1}}, ..., f_{g_{(c-1)}}$$

$$df_{g_1^{(c-1)}} = df_{g_1} ... df_{g_{(c-1)}}$$

$$df_{g_1^{(c-1)} \setminus i} = df_{g_1} ... df_{g_{i-1}} df_{g_{i+1}} ... df_{g_{(c-1)}}$$

$$\int_{f^-_{g_1^{(c-1)}}}^{f^+_{g_1^{(c-1)}}} = \int_{f^-_{g_1}}^{f^+_{g_1}} ... \int_{f^-_{g_{(c-1)}}}^{f^+_{g_{(c-1)}}}$$

$$\int_{f^-_{g_1^{(c-1)} \setminus i}}^{f^+_{g_1^{(c-1)} \setminus i}} = \int_{f^-_{g_1}}^{f^+_{g_1}} ... \int_{f^-_{g_{i-1}}}^{f^+_{g_{i-1}}} \int_{f^-_{g_{i+1}}}^{f^+_{g_{i+1}}} ... \int_{f^-_{g_{(c-1)}}}^{f^+_{g_{(c-1)}}}$$

195

~~The~~

$$\frac{\partial N^j}{\partial t} = 0 \tag{11}$$

as well as the time derivation of Equation (9)~~leads to: :~~

$$\frac{\partial Q_i^j}{\partial t} = N^j \, I_{g_i} \tag{12}$$

Substituting Equation (A16) and $\bar{q}_i = m\ f_i\ \bar{n}$ into Equation (B5), we obtain:

$$\frac{\partial Q_i^j}{\partial t} = \overbrace{\int_{m_k^-}^{m_k^+} \int_{f_{g_1^{(c-1)}}^-}^{f_{g_1^{(c-1)}}^+} m\ f_{g_i} \frac{\partial \bar{n}}{\partial t} dm df_{g_1^{(c-1)}}}^{C} + \int_{m_k^-}^{m_k^+} \int_{f_{g_1^{(c-1)}}^-}^{f_{g_1^{(c-1)}}^+} \bar{n}\ I_{g_i}\ dm df_{g_1^{(c-1)}}$$

$$\overbrace{+ m_k^+ \frac{dm_k^+}{dt} \int_{f_{g_1^{(c-1)}}^-}^{f_{g_1^{(c-1)}}^+} f_{g_i}\ \bar{n}(m_k^+, f_{g_1^{(c-1)}}) df_{g_1^{(c-1)}} - m_k^- \frac{dm_k^-}{dt} \int_{f_{g_1^{(c-1)}}^-}^{f_{g_1^{(c-1)}}^+} f_{g_i}\ \bar{n}(m_k^-, f_{g_1^{(c-1)}}) df_{g_1^{(c-1)}}}^{D}$$

$$+ \sum_{i=1}^{(c-1)} \left[f_{g_i}^+ \frac{df_{g_1^{(c-1)}}^+}{dt} \int_{m_k^-}^{m_k^+} \int_{f_{g_1^{(c-1)}\setminus i}^-}^{f_{g_1^{(c-1)}\setminus i}^+} m\ \bar{n}(m, f_{g_i}^+, f_{g_1^{(c-1)}\setminus i}) dm df_{g_1^{(c-1)}\setminus i} \right.$$

$$\left. - f_{g_i}^- \frac{df_{g_1^{(c-1)}}^-}{dt} \int_{m_k^-}^{m_k^+} \int_{f_{g_1^{(c-1)}\setminus i}^-}^{f_{g_1^{(c-1)}\setminus i}^+} m\ \bar{n}(m, f_{g_i}^-, f_{g_1^{(c-1)}\setminus i}) dm df_{g_1^{(c-1)}\setminus i} \right]$$

Similarly to Equation (B1), it can be proved that $C = -D$, so that Equation (B6) simplifies to:

$$\frac{\partial Q_i^j}{\partial t} = \int_{m_k^-}^{m_k^+} \int_{f_{g_1^{(c-1)}}^-}^{f_{g_1^{(c-1)}}^+} \bar{n}\ I_{g_i}\ dm df_{g_1^{(c-1)}} = N^j\ I_{g_i}$$

Thus, in each section, the change with time of number and mass concentrations is given by Equations (11) and (12).

2.1.4 Numerical implementation

According to Debry and Sportisse (2006), the condensation/evaporation process may have characteristic time-scales of different magnitudes, because the range of particle diameters is large. Such feature induces strong stiffness of the numerical system. As suggested by Debry et al. (2007), the stiff condensation/evaporation equations are solved using the second-order Rosenbrock (ROS2) method (Verwer et al., 1999; Djouad et al., 2002).

In addition, potentially unstable oscillations may occur when a dramatic change of the particle pH occurs. To address this issue, a species flux electro-neutrality constraint (Pilinis et al., 2000; Debry et al., 2007) is applied in SCRAM to ensure the numerical stability of the system.

2.2 Bulk equilibrium and hybrid approaches

~~Bulk equilibrium methods assume an instantaneous thermodynamic equilibrium between the gas and bulk aerosol phases. For semi volatile species, the mass concentration of both gas and bulk aerosol phases after condensation/evaporation are obtained using the forward mode of ISORROPIA for inorganic and the model (Couvidat et al., 2012) for organics. Because time integration is not necessary, the computational cost is significantly reduced compared to the dynamic method. Weighting factors W are designed to distribute the semi volatile bulk aerosol mass across the aerosol distribution (Pandis et al., 1993) . In SCRAM, for each semi volatile species i, we redistribute the bulk aerosol evaporating or condensing mass, $\delta Q_i = Q_i^{\text{after bulk eq.}} - Q_i^{\text{before bulk eq.}}$, between the sections j, using factors that depend on the ratio of the mass transfer rate in the aerosol distribution (Equation 2). Because of the bulk equilibrium assumption, the driving force of $(c_i^g - K_e c_i^{eq})$ is assumed to be the same for all size and composition sections, and the weighting factors are as follows.~~

$$W_i^j = \frac{N_j \, d_p^j f(K_n, \alpha_i)}{\sum_{k=1}^{N_s} N_k \, d_p^k f(K_n, \alpha_i)}$$

~~where N_j is the number concentration of section j and d_p^j is the particle wet diameter of section j. In case of evaporation, these weighting factors may not be appropriate, as they may lead to over evaporation of some species in some sections, i.e. $Q_i^j = Q_i^{\text{before bulk eq.}} + \delta Q_i \times W_i^j < 0$. In the case of over evaporation, we use a weighting scheme that redistributes the total bulk aerosol mass rather than the bulk aerosol evaporating or condensing mass~~

$$W_i^j = \frac{Q_i^j}{\sum_{k=1}^{N_s} Q_i^k}$$

~~and $Q_i^j = Q_i^{\text{after bulk eq.}} \times W_i^j$.~~

2.1.1 Size and composition redistribution

~~In fact, due to their larger ratios between surface area and particle mass, small particles may reach thermodynamic equilibrium much faster than large particles. Particles of diameters larger than 1 could require hours or even days to achieve equilibrium (Wexler and Seinfeld, 1990) , which makes the bulk equilibrium assumption inappropriate for them. In order to maintain both the computational efficiency of the equilibrium method and the accuracy of the dynamic one, a hybrid method is adopted in SCRAM based on the work of Capaldo et al. (2000) and Debry and Sportisse (2006) . This method uses the equilibrium method for small particles ($d_p < 1$) and uses the dynamic method to calculate the mass transfer for larger particles.~~

2.2 ~~Size and composition redistribution~~

By condensation/evaporation, the particles in each size section may grow or shrink. Because the bounds of size sections should be fixed for 3D applications, it is necessary to redistribute number and

mass among the fixed size sections during the simulation after condensation/evaporation. Similarly, the chemical composition also evolves by condensation/evaporation ~~,~~ and an algorithm is needed to identify the particle composition and redistribute it into the correct composition sections.

Two redistribution methods for size sections may be used in SCRAM: the HEMEN (Hybrid of Euler-Mass and Euler-Number) scheme of Devilliers et al. (2013) and the moving diameter scheme of Jacobson (1997). According to Devilliers et al. (2013), both redistribution methods may accurately redistribute mass and number concentrations.

The HEMEN scheme divides particle size sections into two parts: the number is redistributed for sections of mean diameter lower than 100 nm and mass is redistributed for sections of mean diameter greater than 100 nm. The section mean diameters are kept constant and mass concentrations are diagnosed for sections where number is redistributed, while number concentrations are diagnosed for sections where mass is redistributed. The advantage of this scheme is that it is more accurate for number concentrations over the size range where number concentrations are the highest and more accurate for mass concentrations where mass concentrations are the highest. In SCRAM, the algorithm of Devilliers et al. (2013) was modified to take into account the fact that after condensation/evaporation, the diameter of a section may become larger than the upper bound of the next section. In that case, the mean diameter of the section after condensation/evaporation is used to diagnose in which fixed-diameter sections the redistribution is performed. This feature allows us to use larger time steps for condensation/evaporation before redistribution.

In the moving diameter method, although size section bounds are kept fixed, the representative diameter of each size section is allowed to vary. If, after condensation/evaporation, the diameter grows or shrinks outside section bounds, both the mass and number concentrations of the section are redistributed entirely into the new size sections bounding that diameter.

For the composition redistribution, a scheme based on the moving diameter method is applied ~~.~~ (i.e., moving mass fraction). First, after condensation/evaporation, the mass fraction of each species is re-evaluated within each section. For each section, if the new composition does not match the section composition (i.e., if the mass fraction of each species does not fit into the mass fraction bounds of the species for that section), the section ~~which~~ that has a composition that matches the new composition is identified, and both number and mass concentrations of each species are transferred to that section.

2.2 ~~Time resolution of SCRAM~~

The composition redistribution is applied first, followed by the size redistribution for each of the composition sections.

~~In order to~~

2.2 Bulk equilibrium and hybrid approaches

Bulk equilibrium methods assume an instantaneous thermodynamic equilibrium between the gas and bulk-aerosol phases. For semi-volatile species, the mass concentration of both gas and bulk-aerosol phases after condensation/evaporation are obtained using the forward mode of ISORROPIA for inorganics and the H^2O model (Couvidat et al., 2012) for organics. Because time integration is not necessary, the computational cost is significantly reduced compared to the dynamic method. Weighting factors W are designed to distribute the semi-volatile bulk-aerosol mass across the aerosol distribution (Pandis et al., 1993) . In SCRAM, for each semi-volatile species i, we redistribute the bulk aerosol evaporating or condensing mass, $\delta Q_i = Q_i^{\text{after bulk eq.}} - Q_i^{\text{before bulk eq.}}$, between the sections j, using factors that depend on the ratio of the mass transfer rate in the aerosol distribution (Equation 2). Because of the bulk equilibrium assumption, the driving force of $(c_i^g - K_e c_i^{eq})$ is assumed to be the same for all size and composition sections, and the weighting factors are as follows.

$$W_i^j = \frac{N_j \; d_p^j f(K_n, \alpha_i)}{\sum_{k=1}^{N_s} N_k \; d_p^k f(K_n, \alpha_i)} \tag{13}$$

where N_j is the number concentration of section j and d_p^j is the particle wet diameter of section j. In case of evaporation, these weighting factors may not be appropriate, as they may lead to over-evaporation of some species in some sections, i.e. $Q_i^{j\text{ after bulk eq.}} = Q_i^{\text{before bulk eq.}} + \delta Q_i \times W_i^j < 0$. In the case of over-evaporation, we use a weighting scheme that redistributes the total bulk aerosol mass rather than the bulk aerosol evaporating or condensing mass

$$W_i^j = \frac{Q_i^j}{\sum_{k=1}^{N_s} Q_i^k} \tag{14}$$

and $Q_i^{j\text{ after bulk eq.}} = Q_i^{\text{after bulk eq.}} \times W_i^j$.

In fact, due to their larger ratios between surface area and particle mass, small particles may reach thermodynamic equilibrium much faster than large particles. Particles of diameters larger than 1 µm could require hours or even days to achieve equilibrium (Wexler and Seinfeld, 1990) , which makes the bulk equilibrium assumption inappropriate for them. In order to maintain both the computational efficiency of the equilibrium method and the accuracy of the dynamic one, a hybrid method is adopted in SCRAM based on the work of Capaldo et al. (2000) and Debry and Sportisse (2006) . This method uses the equilibrium method for small particles ($d_p < 1$ µm) and uses the dynamic method to calculate the mass transfer for larger particles.

2.3 Overall time integration and operator splitting in SCRAM

In order to develop a system that offers both computational efficiency and numerical stability, we perform operator splitting for changes in number and mass concentrations with time due to emission, coagulation, condensation/evaporation and nucleation, as explained below.

Emissions are first evaluated with an emission time step, which is determined by the characteristic time-scales of emissions obtained from the ratio of emission rates to aerosol concentrations. The

emission time step evolves with time to prevent adding too much emitted mass into the system within one time step. Within each emission time step, coagulation and condensation/evaporation/nucleation are solved and the splitting time step between coagulation and condensation/evaporation/nucleation is forced to be lower than the emission time tep. Time steps are obtained from the characteristic time steps of coagulation (t_{coag}) and condensation/evaporation/nucleation (t_{cond}). The larger of the time steps t_{coag} and t_{cond} determines the time step of splitting between coagulation and condensation/evaporation/nucleation. As coagulation is usually the slower process, the change due to coagulation is first calculated over its time step. Then, ~~the~~ condensation/evaporation/nucleation are solved simultaneously. The change due to condensation/evaporation/nucleation is calculated, using time sub cycles, starting with the sub time step t_{cond}. The next sub time step for condensation/evaporation/nucleation is estimated based on the difference between the first and second order results provided by the ROS2 solver. Redistribution is computed after each time step of splitting of coagulation and condensation/evaporation/nucleation.

When the bulk thermodynamic equilibrium ~~assumption is made,~~ approach is used to solve condensation/evaporation~~is computed with the bulk equilibrium method once per~~ , coagulation then nucleation are solved after each emission time step. The resolution is done as previously explained, except that the dynamic condensation/evaporation solver is disabled: sub time steps are used to solve coagulation and nucleation during one emission time step. ~~In the case of a simulation with the hybrid method for~~ Condensation/evaporation is then solved using the bulk equilibrium approach and the redistribution process is applied after the bulk equilibrium algorithm.

When the hybrid approach is used to solve condensation/evaporation, ~~the change with time of the equilibrium size section is computed~~ a time loop is added with a fixed time step of $600\ s$ ~~, which is larger than~~ outside the emission time ~~steps~~loop to compute bulk equilibrium condensation/evaporation for equilibrium sections. This additional time loop is designed to ensure that bulk equilibrium condensation/evaporation of equilibrium sections is not applied too often, so that ~~enough time is available for the evolution between the background gas concentration and particle surface concentrations for each size section undergoing dynamic mass transfer. Redistribution is computed after each equilibrium time step~~the dynamic condensation/evaporation of dynamic sections has time to evolve. Redistribution is applied after the bulk equilibrium algorithm. Within this time loop, the aerosol dynamics is solved as previously explained using the dynamic condensation / evaporation algorithm for dynamic size sections: emissions are solved followed by coagulation and condensation/ evaporation / nucleation. As in the fully dynamic approach, redistribution is applied after dynamic condensation/ evaporation.

3 Model validation

To validate the model, the change with time of internally- and externally-mixed aerosol models are compared. The simulations use initial conditions for number and mass concentrations that are typical of a regional haze scenario, with a sulphuric acid condensation rate of 5.5 $\mu m^3 cm^{-3}$ per 12 hours (Seigneur et al., 1986; Zhang et al., 1999) (sulphuric acid vapour source of 0.46 $\mu m^3 cm^{-3}$ per hour).

Simulations were conducted for 12 h at a temperature of 298 K and a pressure of 1 ~~ATM~~atm. The original reference simulation (Seigneur et al., 1986; Zhang et al., 1999) was first reproduced for internally-mixed sulphate particles (redistribution is not applied). For the sake of comparison between internally- and externally-mixed simulations, half of the particles were assumed to consist of sulphate (species 1) and the other half of another species of similar physical properties as sulphate (species 2). For internal mixing, the initial particles are all 50% species 1 and 50% species 2; and for external mixing, half of the initial particles are 100% species 1 and the other half are 100% species 2. As both species have the same physical properties, for any given size section, the sum over all composition sections of number and mass concentrations of externally-mixed particles should equal the number and mass concentrations of the internally-mixed particles. Particles were discretised into 100 size sections and 10 composition sections for the externally-mixed case. Figure ~~?? compares the initial mass distributions as a function of both particle size and species 1 mass fraction of the internally- and externally-mixed cases. Figure~~ 1 shows the initial and final distributions for the number and volume concentrations as a function of particle diameters. Both the internally-mixed and externally-mixed results are presented in Figure 1, along with the reference results of Zhang et al. (1999) (500 size sections were used in the original reference simulation). For the externally-mixed simulation, the results were summed up over composition sections to obtain the distributions as a function of particle diameter. As expected, a ~~perfect~~ good match is obtained between internal and external mixing distributions, with ~~a~~ an almost 100% Pearson's correlation coefficient. Furthermore, the accuracy of the SCRAM algorithm is proved by the ~~perfect~~ good match between the results of these simulations and the reference simulation of Zhang et al. (1999). In order to investigate the influence of the composition resolution on simulation results, two additional tests are conducted using 2 and 100 composition bins. The mean mass fraction of species 1 is computed for all particles within each size section, as well as their standard deviations. Figure 2 shows the size distribution of these statistics. The mean mass fraction is barely affected by the different composition resolutions as the condensation rate of sulphate is independent of the particle compositions. However, a different composition resolution does lead to different standard deviation distributions, as only particles with larger fraction difference ($d > 0.2\mu m$ for 2 compositions and $d > 0.09\mu m$ for 10 compositions) can be distinguished from each other under coarser composition resolutions.

Using the same initial conditions and sulphuric acid condensation rate, a second comparison test was performed, with both coagulation and condensation occurring for 12 hours. As the coagulation

algorithm requires size sections to have fixed bounds (Dergaoui et al., 2013), size redistribution was applied for both the internally- and externally-mixed cases using the HEMEN method. As in the first comparison test, Figure 3 shows that there is a ~~perfect~~ good match between the internally- and externally-mixed distributions as a function of particle diameter (no reference simulation was available for these simulations). This test validates the algorithm of SCRAM to simulate jointly the coagulation and condensation of externally-mixed particles.

The mixing states of both internally- and externally-mixed particles at the end of the simulations of the second test are shown in Figure 4. Sulphuric acid condenses to form particulate sulphate (species 1). During the simulation, pure species 2 particles mix with pure sulphate particles by coagulation and condensation of sulphuric acid. Figure 4 shows that, at the end of the simulation, the sulphate mass fraction is greater for particles of lower diameters, because the condensation rate is greater for those particles. Particles with diameters greater than 10 μm remain unmixed. However, the external mixing state provides a more detailed mixing map, from which it is possible to distinguish mixed particles from unmixed ones and to trace the origin of each particle. In this test case where the effect of condensation dominates that of coagulation, most mixed particles are originally pure species 2 particles coated with newly condensed sulphuric acid (Figure 4).

4 Simulation with realistic concentrations

To test the impact of external mixing on aerosol concentrations, simulations of coagulation, condensation/evaporation and nucleation were performed with SCRAM using realistic ambient concentrations and emissions extracted from a simulation performed over Greater Paris for July 2009 during the MEGAPOLI (Megacities: Emissions, urban, regional and Global Atmospheric POLution and climate effects, and Integrated tools for assessment and mitigation) campaign (Couvidat et al., 2013).

4.1 Simulation set-up

Data were extracted from one grid cell of the 3D simulation performed by Couvidat et al. (2013) over Greater Paris. This surface grid cell was chosen because black carbon (BC) emissions are high in that location, due to high traffic emissions. Figure 5 shows the BC emission map at 2 UT, ~~at~~ on 1 July 2009. The highest emission rate is located at the grid cell center of longitude and latitude (2.28° E, 48.88° N), which was selected here to extract the SCRAM simulation input data for emissions, background gas and aerosol concentrations, and initial meteorological conditions (temperature and pressure). In the absence of specific information on individual particle composition, all initial aerosol concentrations extracted from the database were assumed to be 100% mixed (i.e., aged background aerosols).

Simulations start at 2 UT (1 July 2009), i.e., just before the morning peak of traffic emissions, and last 12 hours. As our simulations are 0D, the transport of gases and particles ~~is~~ and the deposition processes are not taken into account~~(i. e., one assume calm conditions).~~. Therefore, emissions accumulate, potentially leading to unrealistically high concentrations. To avoid this artifact, the duration of the emissions was limited to the first 40 min of simulation. This time duration is calculated using the average BC emission rate between 2 UT and 3 UT, so that BC emissions lead to an increase in BC concentrations equal to the difference between BC concentrations after and before the morning traffic peak, i.e., between 6 UT and 2 UT (Figure 6). Besides, gas-phase chemistry (such as SOA formation) is not included in SCRAM, and is expected to be solved separately using a gas-phase chemistry scheme. In the simulations of this work, organics originate either from initial conditions or they are emitted as semi-volatile organic compounds during the simulation. They partition between the gas and the aerosol phases by condensation/evaporation.

The size distribution ranging from 0.001 to 10 μm was discretised into 7 sections with bounds at 0.001, 0.005, 0.01, 0.0398, 0.1585, 0.6310, 2.5119, and 10 μm. As in Couvidat et al. (2013), 31 particulate species were included in our simulations. In order to reduce the computational cost of the externally-mixed simulations, these species were grouped into 5 groups based on their chemical nature~~: the~~ , which influences the formation of particles and their optical properties. Black carbon, organic species, inorganic species and dust are separated. Although sulphate could be separated from nitrate and ammonium for optical properties or for comparisons to observations of mixing state (Healy et al., 2012) , and although chloride and sodium could be grouped together in a marine environment, all inorganic species are grouped together here for the sake of simplicity. However, because the hydrophylic properties of the particles strongly influence their formation and cloud condensation nuclei, hydrophylic and hydrophobic organic species are separated. In summary, the hydrophilic inorganic group (HLI) contains five inorganic species (sodium, sulphate, nitrate, ammonium and chloride); the hydrophilic organic group (HLO) contains 9 hydrophilic surrogate organic species (BiA2D, BiA1D, BiA0D, GLYOXAL, MGLY, BiMT, BiPER, BiDER and BiMGA); the hydrophobic organic group (HBO) contains 14 hydrophobic surrogate organic species (AnBlP, AnBmP, BiBlP, BiBmP, BiNGA, NIT3, BiNIT, AnCLP, SOAlP, SOAmP, SOAhP, POAlP, POAmP and POAhP); the black carbon group (BC) contains only black carbon; and the dust group (DU) contains all the neutral particles made up of soil, dust and fine sand. Refer to Couvidat et al. (2012) for detailed nomenclature of the organic species. For each of the first four groups, the mass fraction of the group over the total mass is discretised into 3 mass fraction sections ($[0.0, 0.2), (0.2, 0.8], (0.8, 1.0]$), leading to 20 possible particle composition sections, as shown in Table 1. Among them, there are 5 unmixed particles and 15 mixed particles. Here unmixed is used in an approximate sense: it means that the mass fraction of one chemical component is high (between 0.8 and 1), while the mass fraction of the other chemical components is low (between 0 and 0.2). The dust mass fraction is not discretised, as it is obtained by mass conservation. Note that although as an example we chose dust

to be the group for which mass fraction is not treated explicitly, another group could be chosen as the group for which mass fraction is not treated explicitly. If all groups need to have their mass fraction treated explicitly, additional composition sections for the last group should be added to the current composition list without any modification to the main structure of the program. The mass fraction of the last group would still be obtained by mass conservation, and the composition section of the particles would be chosen depending on this mass fraction.

In each group, water may also be present, although it is not considered when computing the mass fractions (it is calculated separately with the thermodynamic equilibrium models).

The model memorizes the relationship between each species index and group index, and it stores the mass concentrations separately for each species within each size-composition sections. The total mass concentration of each group is computed from the mass concentration of each species based on the species-group relations, allowing the computation of the mass fraction of each group.

4.2 Aerosol dynamics and mixing state

To understand how initial concentrations mix with emissions, four scenarios were simulated. In ~~the scenario (a~~scenario (A), only emissions are taken into account in the simulation. Only coagulation is added to emissions in scenario (~~b~~B), while only condensation/evaporation(C/E) is added to emissions in scenario (~~c~~C). In ~~the scenario (d~~scenario (D), emissions and all the aerosol dynamic processes are taken into account including nucleation (however, nucleation was not activated during the simulation due to low sulphuric acid gas concentrations).

The mass and number distributions of each chemical composition after 12 hours of simulation are shown in Figures 7 and 8 as a function of particle diameter, as well as their initial distributions in sub-figure (e). Bars with grayscale represent unmixed particles, while bars with colours are mixed particles. Each bar corresponds to a chemical composition index (CI). However, any CI with small number or mass concentrations are not really visible from the plot, so they are regrouped into mixed-other (for mixed CI) and unmixed-other (for unmixed CI) in the plot. The chemical compositions and the CI value associated with ~~color~~ colour bars are listed in Table 1. All emitted particles are unmixed: CI 1 (100% DU) into size section (4-6), CI 3 (100% BC) into size section (3-6). Emissions also involve POA and H_2SO_4 gas-phase emissions.

As shown by the simulation of scenario (~~a~~A), emissions lead to high number concentrations of BC in the sections of low diameters (mostly below 0.631 µm) and to high mass concentrations of dust and BC in the sections of high diameters (mostly above 0.631 µm).

The comparison of scenarios (~~a~~A) and (~~b~~B) shows that coagulation does not affect much mass concentrations, but significantly reduces the number concentrations of particles in the sections of diameters lower than 0.631 µm. Also, due to coagulation, small particles migrated to higher sections. For example, ~~this is illustrated by mixed particles of~~ Figure 8 shows the mixed particles CI 15 ~~that~~ migrated from the third size section to the fourth size section~~(see Figure 8).~~, this might be a result

of the coagulation between CI 3 particles in the third size section and the CI 14 in the fourth size section. Besides, coagulation between CI 5 particles in the third size section may also produce some part of CI 15 in the fourth size section.

As shown by the simulation of scenario (~~c), condensation~~C), C/~~evaporation~~ E leads to high mass and number concentrations of unmixed HBO (CI 6 – mass fraction of HBO (81.2%) above 80% (exact mass fraction of dominate group will be specific within the parentheses right after the group name here after)), increasing the amount of unmixed particles. Organic matter of low and medium volatilities is emitted in the gas phase following Couvidat et al. (2013). This organic matter condenses subsequently on well-mixed particles (CI 14 with mixed HLI ~~and HBO~~(31%) and HBO (41%)), in sufficient amount to increase the mass fraction of HBO (81%) to over 80% and, therefore, transferring particles to the unmixed category CI 6 (these ~~particle~~ particles are not exactly unmixed since up to 20% may correspond to HLI (10%), but a finer composition resolution would be required to analyse their mixed characteristics). The condensation of organic matter on freshly emitted BC particles ~~also occurs. Mixed BC and HBO~~ (CI 3) also occurs, as shown by the mixed BC (26%) and HBO (68%) particles (CI 5) which appear in the third and fourth size sections.

As shown by comparing scenarios (~~a~~A) and (~~b~~B) and scenarios (~~c~~C) and (~~d~~D), coagulation significantly reduces number concentrations. The mass concentrations of fine particles (diameters lower than 0.631 μm) are also reduced. Furthermore, the composition diversity increases. For example, as demonstrated by the difference between scenarios (C) and (D), newly mixed particles of CI 4 (between 20% and 80% of HBO (78% for size 4 and 73% for size 5)) are formed by the coagulation of unmixed particles from CI 6 with others within the fourth and fifth size sections.

Table 2 shows the percentage of mixed particles for each scenario based on both particle number and mass concentrations. ~~In general, the mixed particle percentages based on mass are higher than those based on number. This indicates~~ It seems that large particles ~~, which dominate the mass concentrations,~~ are better mixed than small particles ~~, which dominate the number concentrations. The reason of this difference of mixing state between large and small particles is that emissions lead to high number concentrations of unmixed small particles~~as the mixing percentages of mass are always higher than those of number. However, this phenomenon is specific to this case study; it is caused by the assumption of all initial particles being internally mixed and the initial conditions dominating for large particles due to their low emissions and the short duration of the simulations.

The number/mass mixing percentages after emission only (scenario (~~a~~A)) provide a baseline for the analysis of the three other scenarios. In scenario (~~a~~A), 42% (resp. 83%) of ~~mixed particles~~ the particle number (resp. mass) ~~concentration~~ originates from initial conditions and is mixed, while the remaining ~~unmixed~~ particles are due to emissions and are unmixed. The comparison of scenarios (~~a~~A) and (~~b~~B) shows that coagulation increases the mixing percentages, especially for small particles of high number concentrations. The mass mixing percentages decrease in scenario (~~c~~C) because the condensation of freshly emitted organic matter on large mixed particles leads to particles with a

mass fraction of organic matter (HBO) higher than 80%, i.e. unmixed. When all aerosol dynamic processes are taken into account (scenario (~~d~~D)), only 51% of particle number concentration and 76% of particle mass concentration are mixed. The mixing percentages are greater than those of scenario (~~c~~C), as mixing increases by coagulation, but the mass mixing percentage is lower than in scenario (~~a~~A) (emissions only) because of the strong condensation of HBO emitted in the gas phase.

4.3 External versus internal mixing

To investigate the consequence of the internal mixing hypothesis, a simulation of scenario (~~d~~D) (all aerosol dynamic processes are taken into account) is conducted by assuming all particles to be internally mixed. Externally- and internally-mixed 12-hour simulations lead to a similar total aerosol mass concentration after 12 h (33.09 $\mu g m^{-3}$ for internal mixing and 33.35 $\mu g m^{-3}$ for external mixing) as well as to similar total number concentrations (1.16×10^{10} $\#m^{-3}$ for internal mixing and 1.07×10^{10} $\#m^{-3}$ for external mixing). The number and the species mass distributions are also similar, although external mixing leads to slightly lower ammonium concentrations (2.68 $\mu g m^{-3}$ versus 2.70 $\mu g m^{-3}$), slightly higher nitrate concentrations (3.19 $\mu g m^{-3}$ versus 3.03 $\mu g m^{-3}$) and higher chloride concentrations (0.36 $\mu g m^{-3}$ versus 0.25 $\mu g m^{-3}$).

Figure ~~??~~ 7 (d) and (f) compares the mass distributions and compositions within each size section after 12 h of the internal and external mixing simulations. External mixing provides more detail about the particle mixing state, as within each size section particles have different compositions. For example, in the case of internal mixing, particles in size section 4 (diameter between 0.0398 μm and 0.1585 μm) are all mostly hydrophobic organics (CI 4: HBO (76%) between 20% and 80%). The particle compositions are more detailed in the external mixing simulation: while less than half of the particles are mostly hydrophobic organics (HBO 78%) (CI 4) as in internal mixing, a large amount are unmixed particles (~~TI6: HBO~~ CI 6: HBO (82%) between 80% and 100%), and some are equally mixed with ~~inorganic~~ BC and hydrophobic organics (CI 5). In size section 5, as in the internal mixing simulation, mixed particles dominate (CI 14 - HLI 46%, HBO 36%), but many have a different composition (CI 4 and 5) and some are unmixed HBO 83% (CI 6), BC 91% (CI 3) and dust 90% (CI 1). For particles in size section 6, particles are mixed particles of CI 12 ~~,~~ (HLI 54%,DU 29%), while external mixing also shows that some particles are unmixed (BC 99% (CI 3) and dust 98% (CI 1)) and there are CI 14 (HLI 46%, HBO 35%) particles that originated from size section 5 through coagulation.

4.4 Bulk equilibrium and hybrid approaches

Additional external mixing tests were conducted using the bulk equilibrium and hybrid approaches for ~~condensation~~C/~~evaporation~~ E to evaluate both their accuracy and computational efficiency. In the hybrid approach, the lowest four sections are assumed to be at equilibrium (up to diameters of

0.1585 μm), whereas the other sections undergo dynamic mass transfer between the gas and particle phases .

The accuracy of these approaches is evaluated by comparing the mass and number distributions after 12 hour simulations with the bulk equilibrium or the hybrid approaches to the mass and number distributions computed dynamically (see Figures 9 and 10).

For externally-mixed particles, the dynamic mass distribution is shown in Figure 7(c); the bulk equilibrium and hybrid mass distributions are shown in Figure 9(a) and Figure 9(c), respectively. The dynamic number distribution is shown in Figure 8(c); the bulk equilibrium and hybrid mass distributions are shown in Figure 10(a) and Figure 10(c), respectively. For internally mixed particles, the dynamic mass/number distributions are shown in Figures 9(d) / ~~Figure~~ 10(d) and the bulk equilibrium mass/number distributions in Figures 9(b) / ~~Figures~~ 10(b), respectively.

For internally-mixed particles, the comparisons between Figures 9(b) and 9(d) and between Figures 10(b) and 10(d) indicate that the bulk equilibrium approach leads to significantly different distributions and compositions than the dynamic approach. This result also holds for externally-mixed particles, as shown by the comparisons between Figures 7(c) and 9(a) and between Figures 8(c) and 10(a). For example, more inorganic species condense on particles in the fourth size section (between ~~0.0.0398~~ 0.0398 μm and 0.1585 μm) in the case of bulk equilibrium compared to the fully dynamic case. This section is dominated by CI 14 (HLI 33%, HBO 61%) (equal mixture of inorganic and hydrophobic organics) for bulk equilibrium, instead of CI 6 (HBO 81%) (unmixed hydrophobic organics) for dynamic. Internal and external distributions are similar with the dynamic approach, as well as with the bulk equilibrium approach. Although internal and external compositions are different with the dynamic approach, they are quite similar with the bulk equilibrium approach. However, with the bulk equilibrium approach, similarly to the dynamic approach, unmixed particles of CI 3 (unmixed BC) remain present in most size sections for externally-mixed particles.

The mass and number distributions and compositions obtained with the hybrid approach are similar to the fully dynamic approach. For example, the over-condensation of inorganic species in the fourth size section (leading to particles of CI 14 (HLI 33%, HBO 61%) with bulk equilibrium) is restrained with the hybrid approach, as the fourth size section is computed dynamically, and particles consist of CI 6 (HBO 81%), as with the dynamic approach.

Table 3 shows the computational times (CPU) required for each simulation on a DELL Precision T3500 workstation (the lowest integration time step: 1). External mixing requires more CPU, especially for computing coagulation and dynamic ~~condensation/evaporation (~~C/E~~)~~. The largest difference between internal and external mixing occurs for computing coagulation, which is almost 800 times slower with external mixing. Bulk equilibrium C/E provides a huge economy in CPU time for all simulations compared to dynamic C/E, while the computational advantage of hybrid C/E is more obvious for internal mixing (17 times faster than dynamic C/E) than external mixing (15% ~~times~~ faster than dynamic C/E). This significant speed degradation of the hybrid C/E scheme

in the external mixing case is probably a consequence of small time steps used in the ROS2 solver because of the redistribution among the different composition sections performed after each time step. In other words, it takes CPU time to compute the dynamic distribution among the different composition sections.

5 Conclusions

A new Size-Composition Resolved Aerosol Model (SCRAM) has been developed to simulate the dynamic evolution of externally-mixed particles due to coagulation, condensation/evaporation, and nucleation. The general dynamic equation is discretised for both size and composition. Particle compositions are represented by the combinations of mass fractions, which may be chosen to correspond either to the mass fraction of the different species or to the mass fraction of groups of species (e.g. inorganic, hydrophobic organics...). The total numbers and bounds of the size and composition sections are defined by the user. An automatic classification method is designed within the system to determine all the possible particle compositions based on the combinations of user-defined chemical species or groups and their mass-fraction sections.

The model was first validated by comparison to internally-mixed simulations of condensation / evaporation of sulphuric acid and of condensation / evaporation of sulphuric acid with coagulation. It was also validated for condensation against a reference solution.

The model was applied using realistic concentrations and ~~emissions typical~~ typical emissions of air pollution over Greater Paris, where traffic emissions are high. Initial concentrations were assumed to be internally mixed. Simulations lasted 12 h.

Although internally- and externally-mixed simulations lead to similar particle size distributions, the particle compositions are different. The externally-mixed simulations offer more ~~detail~~ details about particle mixing states within each size section when compared to internally mixed simulations. After 12 h, 49% of number concentrations and 24% of mass concentrations are not mixed. These percentages may be higher in 3D simulations, because initial aerosol concentrations should not be assumed as entirely internally mixed over an urban area. Coagulation is quite efficient at mixing particles, as 52% of number concentrations and 36% of mass concentrations are not mixed if coagulation is not taken into account in the simulation. On the opposite, condensation may decrease the percentage of mixed particles when low-volatility gaseous emissions are high.

Assuming bulk equilibrium when solving condensation/evaporation leads to different distributions and compositions than the dynamic approach under both the internally- and externally-mixed assumptions. Although internally- and externally-mixed assumptions lead to similar compositions with the bulk equilibrium approach, unmixed particles remain when particles are externally mixed, ~~similarly to~~ as observed with the dynamic approach.

Although the simulation of externally mixed particles increases the computational cost, SCRAM offers the possibility to investigate particle mixing state in a comprehensive manner. Besides, its mixing state representation is flexible enough to be modified by users. Better computational performance could be reached with fewer, yet appropriately specified species groups and more optimised composition discretisations. For example, about half of the 20 compositions designed in this work have really low mass concentrations (e.g. see Figures 7, 8, 9 and 10). Those compositions might be dynamically deactivated in the future version of SCRAM to lower computational cost by using an algorithm to skip empty sections during coagulation and C/E processing.

Future work will focus on the optimisation and incorporation of SCRAM into the air quality modelling platform Polyphemus for 3D simulations. In order to investigate its performance in modelling air quality over Greater Paris, model simulation results will be compared to observations (Healy et al., 2012).

Code availability

The SCRAM source code related to this article is available under the URL: http://cerea.enpc.fr/polyphemus/src/scram-1.0.tar.gz , as a supplement package together with Read Me file, where hardware and software requirements, source code files and model output files are fully described.

SCRAM is a free software. You can redistribute it and/or modify it under the terms of the GNU General Public License as published by the Free Software Foundation.

Appendix A: Change of variables for the evolution of number and mass distributions

This appendix describes how to derive the equations of change for the number concentration $\bar{n}$ and mass concentration $\bar{q}$ distributions as a function of the variables $f_1, ..., f_{(c-1)}, m$ used in the external mixing formulation.

To derive the equation of change for $\bar{n}(f_1, ..., f_{(c-1)}, m)$ (Equation 5) from the equation of change for $n(m_1, ..., m_c)$ (Equation 1), we need to perform a change of variables from $m_1, ..., m_c$ to $f_1, ..., f_{(c-1)}, m$

and to compute the $[c \times c]$ Jacobian Matrix $\mathbf{J}(f_1, f_2, \cdots, f_{(c-1)}, m)$

$$\mathbf{J} = \begin{bmatrix} \frac{\partial m_1}{\partial f_1} & \frac{\partial m_1}{\partial f_2} & \cdots & \frac{\partial m_1}{\partial f_{(c-1)}} & \frac{\partial m_1}{\partial m} \\ \frac{\partial m_2}{\partial f_1} & \frac{\partial m_2}{\partial f_2} & \cdots & \frac{\partial m_2}{\partial f_{(c-1)}} & \frac{\partial m_2}{\partial m} \\ \vdots & \vdots & \ddots & \vdots & \vdots \\ \frac{\partial m_{(c-1)}}{\partial f_1} & \frac{\partial m_{(c-1)}}{\partial f_2} & \cdots & \frac{\partial m_{(c-1)}}{\partial f_{(c-1)}} & \frac{\partial m_{(c-1)}}{\partial m} \\ \frac{\partial m_c}{\partial f_1} & \frac{\partial m_c}{\partial f_2} & \cdots & \frac{\partial m_c}{\partial f_{(c-1)}} & \frac{\partial m_c}{\partial m} \end{bmatrix}$$

$$= \begin{bmatrix} m & 0 & \cdots & 0 & f_1 \\ 0 & m & \cdots & 0 & f_2 \\ \vdots & \vdots & \ddots & \vdots & \vdots \\ 0 & 0 & \cdots & m & f_{(c-1)} \\ -m & -m & \cdots & -m & 1 - \sum_{i=1}^{(c-1)} f_i \end{bmatrix} \tag{A1}$$

and the Jacobian inverse matrix:

$$\mathbf{J}^{-1} = \begin{bmatrix} \frac{1-f_1}{m} & -\frac{f_1}{m} & \cdots & -\frac{f_1}{m} & -\frac{f_1}{m} \\ -\frac{f_2}{m} & \frac{1-f_2}{m} & \cdots & -\frac{f_2}{m} & -\frac{f_2}{m} \\ \vdots & \vdots & \ddots & \vdots & \vdots \\ -\frac{f_{(c-1)}}{m} & -\frac{f_{(c-1)}}{m} & \cdots & \frac{1-f_{(c-1)}}{m} & -\frac{f_{(c-1)}}{m} \\ 1 & 1 & \cdots & 1 & 1 \end{bmatrix} \tag{A2}$$

The relationship between n and $\bar{n}$ is

$$n = \frac{\bar{n}}{det(J)} = \frac{\bar{n}}{m^{(c-1)}} \tag{A3}$$

Thus,

$$\frac{\partial n}{\partial t} = \frac{\partial(\frac{\bar{n}}{m^{(c-1)}})}{\partial t} = \frac{1}{m^{(c-1)}} \frac{\partial \bar{n}}{\partial t} \tag{A4}$$

For the right-hand side of Equation (1), the terms $\frac{\partial(I_i n)}{\partial m_i}$ are replaced by terms depending on the new variables, using:

$$\left(\frac{\partial(I_1 n)}{\partial m_1}, \frac{\partial(I_2 n)}{\partial m_2}, \cdots, \frac{\partial(I_c n)}{\partial m_c}\right) = \left(\frac{\partial(I_1 n)}{\partial f_1}, \frac{\partial(I_2 n)}{\partial f_2}, \cdots, \frac{\partial(I_{(c-1)} n)}{\partial f_{(c-1)}}, \frac{\partial(I_c n)}{\partial m}\right) \times \mathbf{J}^{-1} \tag{A5}$$

For $i \in (1, (c-1))$, this leads to:

$$\frac{\partial(I_i n)}{\partial m_i} = \frac{1}{m} \frac{\partial(I_i n)}{\partial f_i} - \sum_{j=1}^{(c-1)} \frac{f_j}{m} \frac{\partial(I_i n)}{\partial f_j} + \frac{\partial(I_i n)}{\partial m} \tag{A6}$$

and for $i = c$:

$$\frac{\partial(I_c n)}{\partial m_c} = -\sum_{j=1}^{(c-1)} \frac{f_j}{m} \frac{\partial(I_c n)}{\partial f_j} + \frac{\partial(I_c n)}{\partial m} \tag{A7}$$

If we replace I_c with $I_0 - \sum_{i=1}^{(c-1)} I_i$ in (A7), we have:

$$\frac{\partial(I_c n)}{\partial m_c} = -\sum_{j=1}^{(c-1)} \frac{f_j}{m} \frac{\partial(I_0 n)}{\partial f_j} + \sum_{i=1}^{(c-1)} \sum_{j=1}^{(c-1)} \frac{f_j}{m} \frac{\partial(I_i n)}{\partial f_j} + \frac{\partial(I_0 n)}{\partial m} - \sum_{i=1}^{(c-1)} \frac{\partial(I_i n)}{\partial m} \tag{A8}$$

The sum of the first $(c-1)$ terms of the right side of Equation (1) may be written as follows.

$$\sum_{i=1}^{(c-1)} \frac{\partial(I_i n)}{\partial m_i} = \frac{1}{m} \sum_{i=1}^{(c-1)} \frac{\partial(I_i n)}{\partial f_i} - \sum_{i=1}^{(c-1)} \sum_{j=1}^{(c-1)} \frac{f_j}{m} \frac{\partial(I_i n)}{\partial f_j} + \sum_{i=1}^{(c-1)} \frac{\partial(I_i n)}{\partial m} \tag{A9}$$

The right-hand side of Equation (1) becomes

$$-\sum_{i=1}^{c} \frac{\partial(I_i n)}{\partial m_i} = -\sum_{i=1}^{(c-1)} \frac{\partial(I_i n)}{\partial m_i} - \frac{\partial(I_c n)}{\partial m_c} = -\frac{1}{m} \sum_{i=1}^{(c-1)} \frac{\partial(I_i n)}{\partial f_i} + \sum_{i=1}^{(c-1)} \frac{f_i}{m} \frac{\partial(I_0 n)}{\partial f_i} - \frac{\partial(I_0 n)}{\partial m} \tag{A10}$$

If we denote $H_i = \dfrac{\partial f_i}{\partial t}$, then I_i may be written as follows.

$$I_i = \frac{\partial m_i}{\partial t} = \frac{\partial(m f_i)}{\partial t} = m \frac{\partial f_i}{\partial t} + f_i \frac{\partial m}{\partial t} = m H_i + f_i I_0 \tag{A11}$$

Replacing I_i by (A11) in (A10) and using $\dfrac{\partial m}{\partial f_i} = 0$,

$$\begin{aligned} -\sum_{i=1}^{c} \frac{\partial(I_i n)}{\partial m_i} &= -\frac{1}{m} \sum_{i=1}^{(c-1)} \frac{\partial(m H_i n + f_i I_0 n)}{\partial f_i} + \sum_{i=1}^{(c-1)} \frac{f_i}{m} \frac{\partial(I_0 n)}{\partial f_i} - \frac{\partial(I_0 n)}{\partial m} \\ &= -\sum_{i=1}^{(c-1)} \frac{\partial(H_i n)}{\partial f_i} - \frac{(c-1)}{m} I_0 n - \frac{\partial(I_0 n)}{\partial m} \end{aligned} \tag{A12}$$

Replacing n with $\dfrac{\bar{n}}{m^{(c-1)}}$ in Equation (1) and using (A12), we have

$$\begin{aligned} \frac{1}{m^{(c-1)}} \frac{\partial \bar{n}}{\partial t} &= -\sum_{i=1}^{(c-1)} \frac{\partial(H_i \frac{\bar{n}}{m^{(c-1)}})}{\partial f_i} - \frac{(c-1)}{m^c} I_0 \bar{n} - \frac{\partial(I_0 \frac{\bar{n}}{m^{(c-1)}})}{\partial m} \\ &= -\frac{1}{m^{(c-1)}} \sum_{i=1}^{(c-1)} \frac{\partial(H_i \bar{n})}{\partial f_i} - \frac{1}{m^{(c-1)}} \frac{\partial(I_0 \bar{n})}{\partial m} \end{aligned} \tag{A13}$$

and the equation of change for $\bar{n}$ is finally

$$\frac{\partial \bar{n}}{\partial t} = -\sum_{i=1}^{(c-1)} \frac{\partial(H_i \bar{n})}{\partial f_i} - \frac{\partial(I_0 \bar{n})}{\partial m} \tag{A14}$$

The equation of change for the mass distribution $q_i = n\, m_i$ of species i is derived as follows.

$$\frac{\partial q_i}{\partial t} = \frac{\partial n\, m_i}{\partial t} = -m_i \frac{\partial n}{\partial t} + n\, I_i \tag{A15}$$

And the equation of change for $\bar{q}_i$ is obtained using $n = \dfrac{\bar{n}}{m^{(c-1)}}$, $q_i = \dfrac{\bar{q}_i}{m^{(c-1)}}$ and $m_i = m\, f_i$

$$\frac{\partial \bar{q}_i}{\partial t} = -m\, f_i \frac{\partial \bar{n}}{\partial t} + \bar{n}\, I_i \tag{A16}$$

Appendix B: The time derivation of Equation (10) and (9)

The time derivation of Equation (10) leads to:

$$\begin{aligned}
\frac{\partial N^j}{\partial t} = & \overbrace{\int_{m_k^-}^{m_k^+}\int_{f_{g_1}^-}^{f_{g_1}^+}\cdots\int_{f_{g_{(c-1)}}^-}^{f_{g_{(c-1)}}^+}\frac{\partial \bar{n}}{\partial t}\, dm df_{g_1},...,df_{g_{(c-1)}}}^{A} \\
& \overbrace{+\frac{dm_k^+}{dt}\int_{f_{g_1}^-}^{f_{g_1}^+}\cdots\int_{f_{g_{(c-1)}}^-}^{f_{g_{(c-1)}}^+}\bar{n}(m_k^+, f_{g_1},...,f_{g_{(c-1)}})df_{g_1},...,df_{g_{(c-1)}} - \frac{dm_k^-}{dt}\int_{f_{g_1}^-}^{f_{g_1}^+}\cdots\int_{f_{g_{(c-1)}}^-}^{f_{g_{(c-1)}}^+}\bar{n}(m_k^-, f_{g_1},...,f_{g_{(c-1)}})df_{g_1},...,df_{g_{(c-1)}}}^{B} \\
& + \sum_{i=1}^{(c-1)}\left[\frac{df_{g_i}^+}{dt}\int_{m_k^-}^{m_k^+}\int_{f_{g_1}^-}^{f_{g_1}^+}\cdots\int_{f_{g_{i-1}}^-}^{f_{g_{i-1}}^+}\int_{f_{g_{i+1}}^-}^{f_{g_{i+1}}^+}\cdots\int_{f_{g_{(c-1)}}^-}^{f_{g_{(c-1)}}^+}\bar{n}(m, f_{g_1},...,f_{g_{i-1}}, f_{g_i^+}, f_{g_{i+1}},...,f_{g_{(c-1)}})dm df_{g_1}...df_{g_{i-1}}df_{g_{i+1}}...df_{g_{(c-1)}}\right. \\
& \left. - \frac{df_{g_i}^-}{dt}\int_{m_k^-}^{m_k^+}\int_{f_{g_1}^-}^{f_{g_1}^+}\cdots\int_{f_{g_{i-1}}^-}^{f_{g_{i-1}}^+}\int_{f_{g_{i+1}}^-}^{f_{g_{i+1}}^+}\cdots\int_{f_{g_{(c-1)}}^-}^{f_{g_{(c-1)}}^+}\bar{n}(m, f_{g_1},...,f_{g_{i-1}}, f_{g_i^-}, f_{g_{i+1}},...,f_{g_{(c-1)}})dm df_{g_1}...df_{g_{i-1}}df_{g_{i+1}}...df_{g_{(c-1)}}\right]
\end{aligned} \tag{B1}$$

Replacing $\dfrac{\partial \bar{n}}{\partial t}(m, f_{g_1},..., f_{g_{(c-1)}})$ by Equation (5), we have

$$A = \int_{m_k^-}^{m_k^+}\int_{f_{g_1}^-}^{f_{g_1}^+}\cdots\int_{f_{g_{(c-1)}}^-}^{f_{g_{(c-1)}}^+}\left[-\frac{\partial(I_0 n)}{\partial m} - \sum_{x=1}^{(c-1)}\frac{\partial(H_{g_x} n)}{\partial f_{g_x}}\right] dm df_{g_1}...df_{g_{(c-1)}} \tag{B2}$$

and using $I_0 = \frac{dm}{dt}$, $H_{g_i} = \frac{df_{g_i}}{dt}$ and $\frac{\partial f_{g_i}}{\partial f_{g_l}} = 0$ when $i \neq l$

$$A = -\left\{ \frac{dm_k^+}{dt} \int_{f_{g_1}^-}^{f_{g_1}^+} ... \int_{f_{g_{(c-1)}}^-}^{f_{g_{(c-1)}}^+} \bar{n}(m_k^+, f_{g_1}, ..., f_{g_{(c-1)}}) dm df_{g_1} ... df_{g_{(c-1)}} - \frac{dm_k^-}{dt} \int_{f_{g_1}^-}^{f_{g_1}^+} ... \int_{f_{g_{(c-1)}}^-}^{f_{g_{(c-1)}}^+} \bar{n}(m_k^-, f_{g_1}, ..., f_{g_{(c-1)}}) dm df_{g_1} ... df_{g_{(c-1)}} \right.$$

$$+ \sum_{i=1}^{(c-1)} \left[\frac{df_{g_i}^+}{dt} \int_{m_k^-}^{m_k^+} \int_{f_{g_1}^-}^{f_{g_1}^+} ... \int_{f_{g_{i-1}}^-}^{f_{g_{i-1}}^+} \int_{f_{g_{i+1}}^-}^{f_{g_{i+1}}^+} ... \int_{f_{g_{(c-1)}}^-}^{f_{g_{(c-1)}}^+} \bar{n}(m, f_{g_1}, ..., f_{g_{i-1}}, f_{g_i^+}, f_{g_{i+1}}, ..., f_{g_{(c-1)}}) dm df_{g_1} ... df_{g_{i-1}} df_{g_{i+1}} ... df_{g_{(c-1)}} \right.$$

$$\left. \left. - \frac{df_{g_i}^-}{dt} \int_{m_k^-}^{m_k^+} \int_{f_{g_1}^-}^{f_{g_1}^+} ... \int_{f_{g_{i-1}}^-}^{f_{g_{i-1}}^+} \int_{f_{g_{i+1}}^-}^{f_{g_{i+1}}^+} ... \int_{f_{g_{(c-1)}}^-}^{f_{g_{(c-1)}}^+} \bar{n}(m, f_{g_1}, ..., f_{g_{i-1}}, f_{g_i^-}, f_{g_{i+1}}, ..., f_{g_{(c-1)}}) dm df_{g_1} ... df_{g_{i-1}} df_{g_{i+1}} ... df_{g_{(c-1)}} \right] \right\}$$

(B3)

So $A = -B$, thus

$$\frac{\partial N^j}{\partial t} = (A + B) = 0 \tag{B4}$$

which is expected since condensation/evaporation does not affect the total number of particles.

Similarly, an equation of change can be derived for Q_i^j. In order to simplify the writing of the equations, the following abbreviations are introduced:

$$f_{g_1^{(c-1)}} = f_{g_1}, ..., f_{g_{(c-1)}}$$

$$f_{g_1^{(c-1)} \setminus i} = f_{g_1}, ..., f_{g_{i-1}}, f_{g_{i+1}}, ..., f_{g_{(c-1)}}$$

$$df_{g_1^{(c-1)}} = df_{g_1} ... df_{g_{(c-1)}}$$

$$df_{g_1^{(c-1)} \setminus i} = df_{g_1} ... df_{g_{i-1}} df_{g_{i+1}} ... df_{g_{(c-1)}}$$

$$\int_{f_{g_1^{(c-1)}}^-}^{f_{g_1^{(c-1)}}^+} = \int_{f_{g_1}^-}^{f_{g_1}^+} ... \int_{f_{g_{(c-1)}}^-}^{f_{g_{(c-1)}}^+}$$

$$\int_{f_{g_1^{(c-1)} \setminus i}^-}^{f_{g_1^{(c-1)} \setminus i}^+} = \int_{f_{g_1}^-}^{f_{g_1}^+} ... \int_{f_{g_{i-1}}^-}^{f_{g_{i-1}}^+} \int_{f_{g_{i+1}}^-}^{f_{g_{i+1}}^+} ... \int_{f_{g_{(c-1)}}^-}^{f_{g_{(c-1)}}^+}$$

The time derivation of Equation (9) leads to:

$$\frac{\partial Q_i^j}{\partial t} = \int_{m_k^-}^{m_k^+} \int_{f_{g_1^{(c-1)}}^-}^{f_{g_1^{(c-1)}}^+} \frac{\partial \bar{q}_i}{\partial t} dm df_{g_1^{(c-1)}}$$
$$+ \frac{dm_k^+}{dt} \int_{f_{g_1^{(c-1)}}^-}^{f_{g_1^{(c-1)}}^+} \bar{q}_i(m_k^+, f_{g_1^{(c-1)}}) df_{g_1^{(c-1)}} - \frac{dm_k^-}{dt} \int_{f_{g_1^{(c-1)}}^-}^{f_{g_1^{(c-1)}}^+} \bar{q}_i(m_k^-, f_{g_1^{(c-1)}}) df_{g_1^{(c-1)}}$$
$$+ \sum_{i=1}^{(c-1)} \left[\frac{df_{g_1^{(c-1)}}^+}{dt} \int_{m_k^-}^{m_k^+} \int_{f_{g_1^{(c-1)}\setminus i}^-}^{f_{g_1^{(c-1)}\setminus i}^+} \bar{q}_i(m, f_{g_i}^+, f_{g_1^{(c-1)}\setminus i}) dm df_{g_1^{(c-1)}\setminus i} \right.$$
$$\left. - \frac{df_{g_1^{(c-1)}}^-}{dt} \int_{m_k^-}^{m_k^+} \int_{f_{g_1^{(c-1)}\setminus i}^-}^{f_{g_1^{(c-1)}\setminus i}^+} \bar{q}_i(m, f_{g_i}^-, f_{g_1^{(c-1)}\setminus i}) dm df_{g_1^{(c-1)}\setminus i} \right] \quad \text{(B5)}$$

Substituting Equation (A16) and $\bar{q}_i = m\, f_i\, \bar{n}$ into Equation (B5), we obtain:

$$\frac{\partial Q_i^j}{\partial t} = \overbrace{\int_{m_k^-}^{m_k^+} \int_{f_{g_1^{(c-1)}}^-}^{f_{g_1^{(c-1)}}^+} m\, f_{g_i} \frac{\partial \bar{n}}{\partial t} dm df_{g_1^{(c-1)}}}^{C} + \int_{m_k^-}^{m_k^+} \int_{f_{g_1^{(c-1)}}^-}^{f_{g_1^{(c-1)}}^+} \bar{n}\, I_{g_i}\, dm df_{g_1^{(c-1)}}$$
$$\overbrace{+ m_k^+ \frac{dm_k^+}{dt} \int_{f_{g_1^{(c-1)}}^-}^{f_{g_1^{(c-1)}}^+} f_{g_i}\, \bar{n}(m_k^+, f_{g_1^{(c-1)}}) df_{g_1^{(c-1)}} - m_k^- \frac{dm_k^-}{dt} \int_{f_{g_1^{(c-1)}}^-}^{f_{g_1^{(c-1)}}^+} f_{g_i}\, \bar{n}(m_k^-, f_{g_1^{(c-1)}}) df_{g_1^{(c-1)}}}^{D}$$
$$+ \sum_{i=1}^{(c-1)} \left[f_{g_i}^+ \frac{df_{g_1^{(c-1)}}^+}{dt} \int_{m_k^-}^{m_k^+} \int_{f_{g_1^{(c-1)}\setminus i}^-}^{f_{g_1^{(c-1)}\setminus i}^+} m\, \bar{n}(m, f_{g_i}^+, f_{g_1^{(c-1)}\setminus i}) dm df_{g_1^{(c-1)}\setminus i} \right.$$
$$\left. - f_{g_i}^- \frac{df_{g_1^{(c-1)}}^-}{dt} \int_{m_k^-}^{m_k^+} \int_{f_{g_1^{(c-1)}\setminus i}^-}^{f_{g_1^{(c-1)}\setminus i}^+} m\, \bar{n}(m, f_{g_i}^-, f_{g_1^{(c-1)}\setminus i}) dm df_{g_1^{(c-1)}\setminus i} \right] \quad \text{(B6)}$$

Similarly to Equation (B1), it can be proved that $C = -D$, so that Equation (B6) simplifies to:

$$\frac{\partial Q_i^j}{\partial t} = \int_{m_k^-}^{m_k^+} \int_{f_{g_1^{(c-1)}}^-}^{f_{g_1^{(c-1)}}^+} \bar{n}\, I_{g_i}\, dm df_{g_1^{(c-1)}} = N^j\, I_{g_i} \tag{B7}$$

Thus, in each section, the change with time of number and mass concentrations is given by Equations (B4) and (B7).

Acknowledgements. The authors gratefully acknowledge Hilel Dergaoui (INRA) for providing his original code of coagulation process and Edouard Debry (INERIS) for ~~optimizing~~ optimising the computation of coagulation ~~repartition~~ distribution coefficients. We also would like to thank Florian Couvidat (INERIS) for his support on the implementation of his H^2O model into SCRAM as well as Stéphanie Deschamps (CEREA) who helped to improve the size redistribution algorithm.

References

Bauer, S., Wright, D., Koch, D., Lewis, E., McGraw, R., Chang, L.-S., Schwartz, S., and Ruedy, R.: MATRIX (Multiconfiguration Aerosol TRacker of mIXing state): an aerosol microphysical module for global atmospheric models, Atmospheric Chemistry and Physics, 8, 6003–6035, 2008.

Binkowski, F. S. and Roselle, S. J.: Models-3 Community Multiscale Air Quality (CMAQ) model aerosol component 1. Model description, Journal of Geophysical Research: Atmospheres (1984–2012), 108, 2003.

Capaldo, K., Pilinis, C., and Pandis, S. N.: A computationally efficient hybrid approach for dynamic gas/aerosol transfer in air quality models, Atmospheric Environment, 34, 3617–3627, 2000.

Couvidat, F., Debry, É., Sartelet, K., and Seigneur, C.: A hydrophilic/hydrophobic organic (H2O) aerosol model: Development, evaluation and sensitivity analysis, Journal of Geophysical Research: Atmospheres (1984–2012), 117, 2012.

Couvidat, F., Kim, Y., Sartelet, K., Seigneur, C., Marchand, N., and Sciare, J.: Modeling secondary organic aerosol in an urban area: application to Paris, France, Atmospheric Chemistry and Physics, 13, 983–996, 2013.

Dahneke, B.: Simple kinetic theory of Brownian diffusion in vapors and aerosols, in: Theory of Dispersed Multiphase Flow, pp. 97–133, Academic Press, 1983.

Deboudt, K., Flament, P., Choël, M., Gloter, A., Sobanska, S., and Colliex, C.: Mixing state of aerosols and direct observation of carbonaceous and marine coatings on African dust by individual particle analysis, Journal of Geophysical Research: Atmospheres (1984–2012), 115, 2010.

Debry, E. and Sportisse, B.: Reduction of the condensation/evaporation dynamics for atmospheric aerosols: Theoretical and numerical investigation of hybrid methods, Journal of Aerosol Science, 37, 950–966, 2006.

Debry, E., Fahey, K., Sartelet, K., Sportisse, B., and Tombette, M.: Technical Note: A new SIze REsolved Aerosol Model (SIREAM), Atmospheric Chemistry and Physics, 7, 1537–1547, 2007.

Dergaoui, H., Sartelet, K. N., Debry, É., and Seigneur, C.: Modeling coagulation of externally mixed particles: Sectional approach for both size and chemical composition, Journal of Aerosol Science, 58, 17 – 32, 2013.

Devilliers, M., Debry, É., Sartelet, K., and Seigneur, C.: A new algorithm to solve condensation/evaporation for ultra fine, fine, and coarse particles, Journal of Aerosol Science, 55, 116–136, 2013.

Djouad, R., Sportisse, B., and Audiffren, N.: Numerical simulation of aqueous-phase atmospheric models: use of a non-autonomous Rosenbrock method, Atmospheric Environment, 36, 873–879, 2002.

EPA, D.: Integrated science assessment for particulate matter, US Environmental Protection Agency Washington, DC, 2009.

Gelbard, F. and Seinfeld, J. H.: Simulation of multicomponent aerosol dynamics, Journal of colloid and Interface Science, 78, 485–501, 1980.

Healy, R., Sciare, J., Poulain, L., Kamili, K., Merkel, M., Müller, T., Wiedensohler, A., Eckhardt, S., Stohl, A., Sarda-Estève, R., et al.: Sources and mixing state of size-resolved elemental carbon particles in a European megacity: Paris, Atmospheric Chemistry and Physics, 12, 1681–1700, 2012.

Hughes, L. S., Allen, J. O., Bhave, P., Kleeman, M. J., Cass, G. R., Liu, D.-Y., Fergenson, D. P., Morrical, B. D., and Prather, K. A.: Evolution of atmospheric particles along trajectories crossing the Los Angeles basin, Environmental science & technology, 34, 3058–3068, 2000.

Jacobson, M.: Analysis of aerosol interactions with numerical techniques for solving coagulation, nucleation, condensation, dissolution, and reversible chemistry among multiple size distributions, Journal of Geophysical Research, 107, 1327–1338, 2002.

Jacobson, M. Z.: Development and application of a new air pollution modeling system—II. Aerosol module structure and design, Atmospheric Environment, 31, 131–144, 1997.

Jacobson, M. Z.: Strong radiative heating due to the mixing state of black carbon in atmospheric aerosols, Nature, 409, 695–697, 2001.

Jacobson, M. Z., Turco, R. P., Jensen, E. J., and Toon, O. B.: Modeling coagulation among particles of different composition and size, Atmospheric Environment, 28, 1327–1338, 1994.

Kleeman, M. J. and Cass, G. R.: A 3D Eulerian source-oriented model for an externally mixed aerosol, Environmental science & technology, 35, 4834–4848, 2001.

Kleeman, M. J., Cass, G. R., and Eldering, A.: Modeling the airborne particle complex as a source-oriented external mixture, Journal of Geophysical Research: Atmospheres (1984–2012), 102, 21 355–21 372, 1997.

Leck, N. and Svensson, E.: Importance of aerosol composition and mixing state for cloud droplet activation in the high Arctic, Atmospheric Chemistry and Physics Discussion, 14, 21 223–21 283, 2014.

Lesins, G., Chylek, P., and Lohmann, U.: A study of internal and external mixing scenarios and its effect on aerosol optical properties and direct radiative forcing, Journal of Geophysical Research: Atmospheres (1984–2012), 107, AAC–5, 2002.

Lu, J. and Bowman, F. M.: A detailed aerosol mixing state model for investigating interactions between mixing state, semivolatile partitioning, and coagulation, Atmospheric Chemistry and Physics, 10, 4033–4046, 2010.

Mallet, M., Roger, J., Despiau, S., Putaud, J., and Dubovik, O.: A study of the mixing state of black carbon in urban zone, Journal of Geophysical Research: Atmospheres (1984–2012), 109, 2004.

McMurry, P. H.: A review of atmospheric aerosol measurements, Atmospheric Environment, 34, 1959–1999, 2000.

Myhre, G., Samset, B., Schulz, M., Balkanski, Y., Bauer, S., Berntsen, T., Bian, H., Bellouin, N., Chin, M., Diehl, T., et al.: Radiative forcing of the direct aerosol effect from AeroCom Phase II simulations, Atmospheric Chemistry and Physics, 13, 1853–1877, 2013.

Nenes, A., Pandis, S. N., and Pilinis, C.: ISORROPIA: A new thermodynamic equilibrium model for multiphase multicomponent inorganic aerosols, Aquatic geochemistry, 4, 123–152, 1998.

Oshima, N., Koike, M., Zhang, Y., Kondo, Y., Moteki, N., Takegawa, N., and Miyazaki, Y.: Aging of black carbon in outflow from anthropogenic sources using a mixing state resolved model: Model development and evaluation, Journal of Geophysical Research: Atmospheres (1984–2012), 114, 2009.

Pandis, S. N., Wexler, A. S., and Seinfeld, J. H.: Secondary organic aerosol formation and transport—II. Predicting the ambient secondary organic aerosol size distribution, Atmospheric Environment. Part A. General Topics, 27, 2403–2416, 1993.

Pascal, M., Corso, M., Chanel, O., Declercq, C., Badaloni, C., Cesaroni, G., Henschel, S., Meister, K., Haluza, D., Martin-Olmedo, P., et al.: Assessing the public health impacts of urban air pollution in 25 European cities: Results of the Aphekom project, Science of the Total Environment, 449, 390–400, 2013.

Pilinis, C., Capaldo, K., Nenes, A., and Pandis, S.: MADM-A new multicomponent aerosol dynamics model, Aerosol Science & Technology, 32, 482–502, 2000.

Riemer, N., West, M., Zaveri, R. A., and Easter, R. C.: Simulating the evolution of soot mixing state with a particle-resolved aerosol model, Journal of Geophysical Research, 114, D09 202, 2009.

Sartelet, K., Debry, E., Fahey, K., Roustan, Y., Tombette, M., and Sportisse, B.: Simulation of aerosols and gas-phase species over Europe with the Polyphemus system: Part I Model-to-data comparison for 2001, Atmospheric Environment, 41, 6116–6131, 2007.

Seigneur, C., Hudischewskyj, a. B., Seinfeld, J. H., Whitby, K. T., Whitby, E. R., Brock, J. R., and Barnes, H. M.: Simulation of Aerosol Dynamics: A Comparative Review of Mathematical Models, Aerosol Science and Technology, 5, 205–222, 1986.

Stier, P., Feichter, J., Kinne, S., Kloster, S., Vignati, E., Wilson, J., Ganzeveld, L., Tegen, I., Werner, M., Balkanski, Y., et al.: The aerosol-climate model ECHAM5-HAM, Atmospheric Chemistry and Physics, 5, 1125–1156, 2005.

Vehkamäki, H., Kulmala, M., Napari, I., Lehtinen, K. E., Timmreck, C., Noppel, M., and Laaksonen, A.: An improved parameterization for sulfuric acid–water nucleation rates for tropospheric and stratospheric conditions, Journal of Geophysical Research: Atmospheres (1984–2012), 107, AAC–3, 2002.

Verwer, J. G., Spee, E., Blom, J., and Hundsdorfer, W.: A second-order Rosenbrock method applied to photochemical dispersion problems, SIAM Journal on Scientific Computing, 20, 1456–1480, 1999.

Wexler, A. S. and Seinfeld, J. H.: The distribution of ammonium salts among a size and composition dispersed aerosol, Atmospheric Environment. Part A. General Topics, 24, 1231–1246, 1990.

Whitby, E. R. and McMurry, P. H.: Modal aerosol dynamics modeling, Aerosol Science and Technology, 27, 673–688, 1997.

Zhang, Y., Seigneur, C., Seinfeld, J. H., Jacobson, M. Z., and Binkowski, F. S.: Simulation of Aerosol Dynamics: A Comparative Review of Algorithms Used in Air Quality Models, Aerosol Science and Technology, 31, 487–514, 1999.

Zhang, Y., Pun, B., Vijayaraghavan, K., Wu, S.-Y., Seigneur, C., Pandis, S. N., Jacobson, M. Z., Nenes, A., and Seinfeld, J. H.: Development and application of the model of aerosol dynamics, reaction, ionization, and dissolution (MADRID), Journal of Geophysical Research: Atmospheres (1984–2012), 109, 2004.

Zhang, Y., McMurry, P. H., Yu, F., and Jacobson, M. Z.: A comparative study of nucleation parameterizations: 1. Examination and evaluation of the formulations, Journal of Geophysical Research: Atmospheres (1984–2012), 115, 2010.

~~Initial distribution: particle mass concentration as a function of diameter and mass fraction of species 1.~~

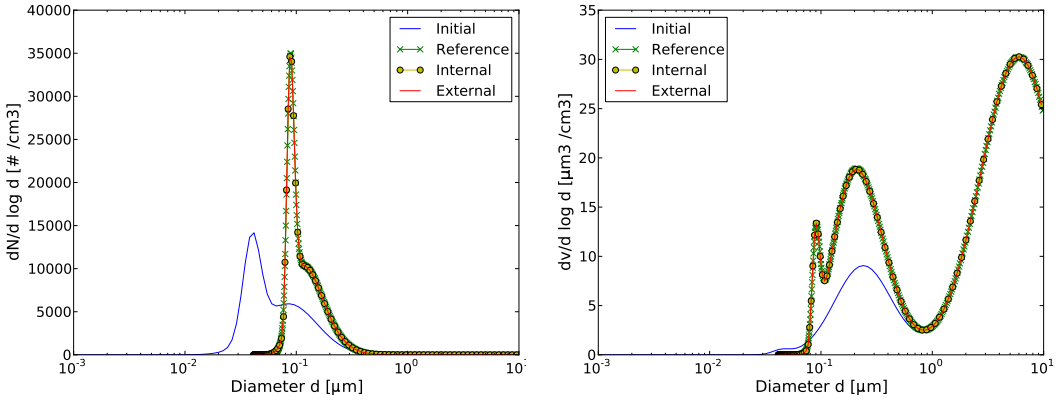

(a) Number distribution (b) Volume distribution

Figure 1. Simulation of condensation for hazy conditions: initial distribution and after 12 hours.

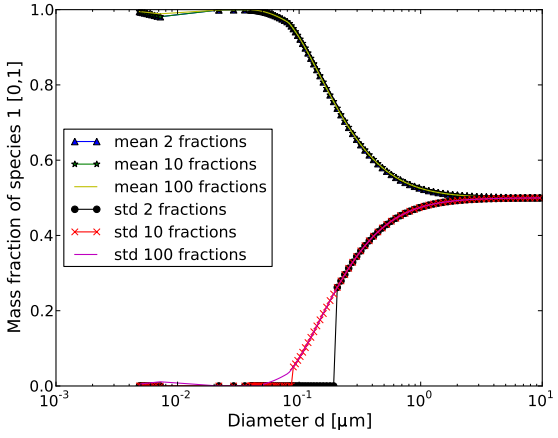

Figure 2. Mean and standard deviations of species 1 mass fraction as functions of particle diameter using 2, 10 and 100 composition sections.

~~Mass distributions as a function of particle diameter and composition for the internal and external mixing cases.~~

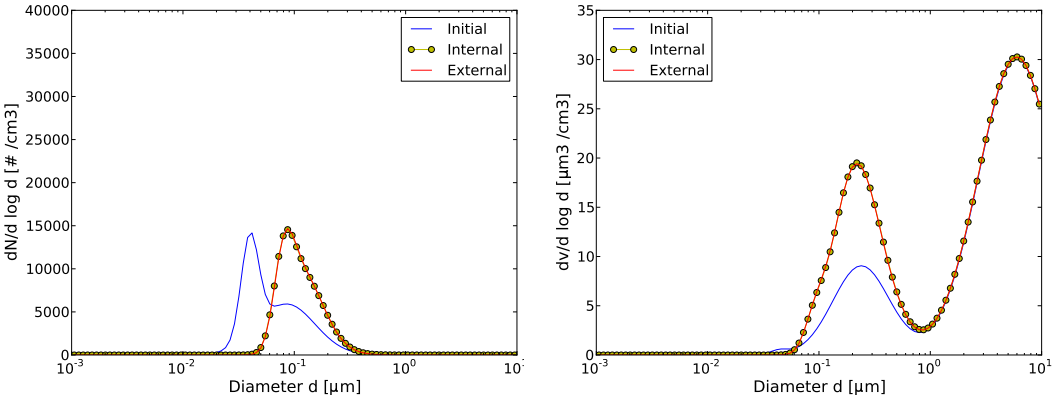

(a) Number distribution (b) Volume distribution

Figure 3. Simulation of both coagulation and condensation for hazy conditions: initial distribution and after 12 hours.

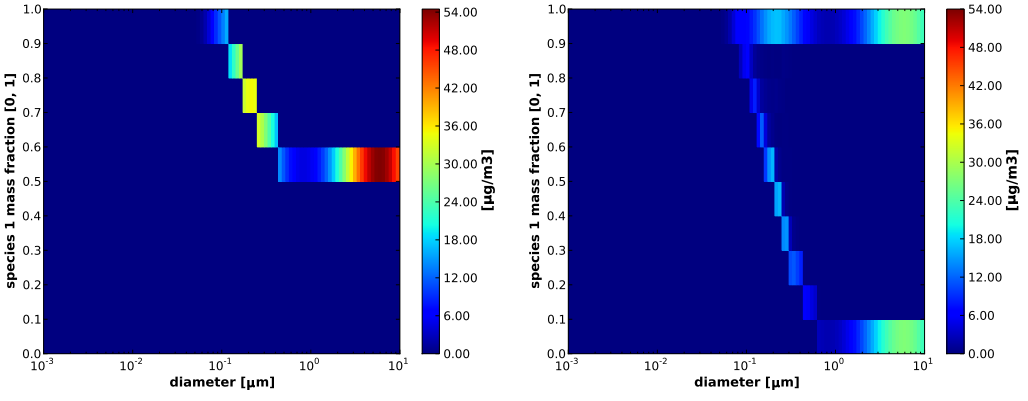

(a) Internal mixing (b) External mixing

Figure 4. Distribution after 12 hours: particle mass concentration as a function of diameter and mass fraction of species 1.

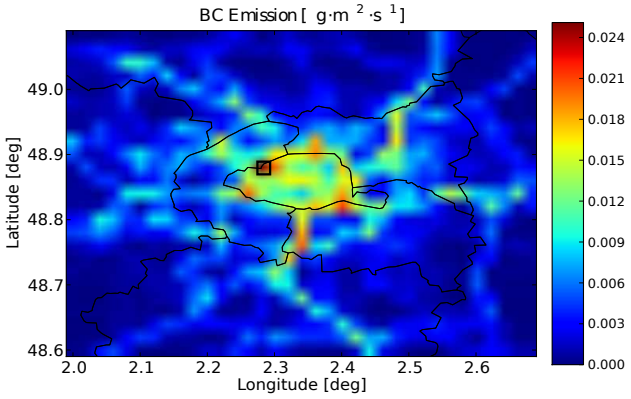

Figure 5. BC emissions over Greater Paris at 2 UT, 1 July 2009.

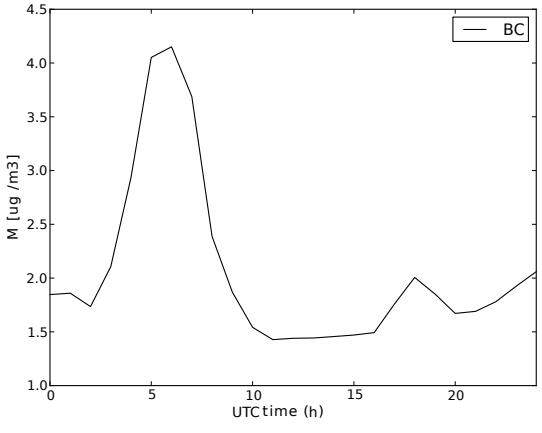

Figure 6. Transprt BC concentrations profile of on 1 July 2009.

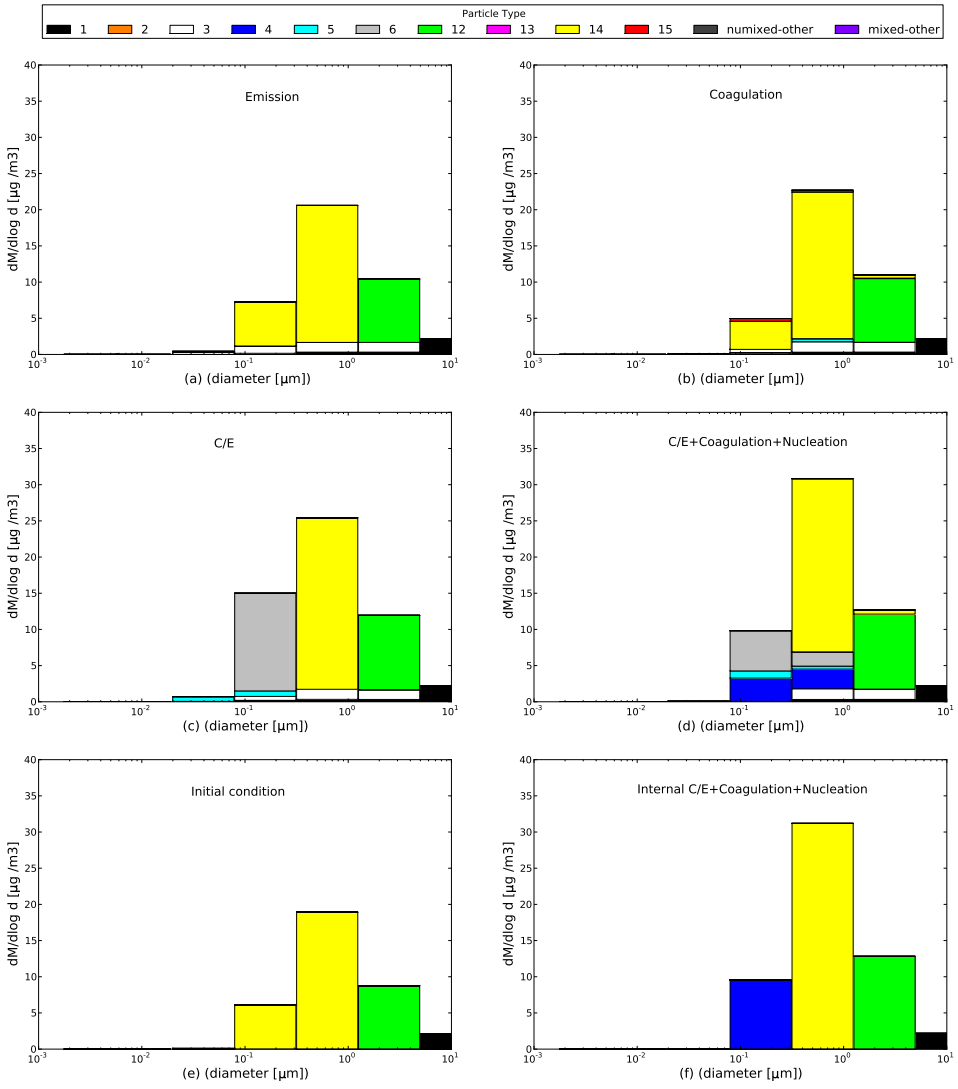

Figure 7. ~~Mass~~ Result mass distributions of externally-mixed particles as a function of particle diameter for the different chemical compositions for 6 different simulation scenarios: (a) Emission only; (b) Emission+Coagulation; (c) Emission+C/E; (d) Emission+Coagulation+C/E+nucleation; (e) Initial Condition; (f) Internal mixing result.

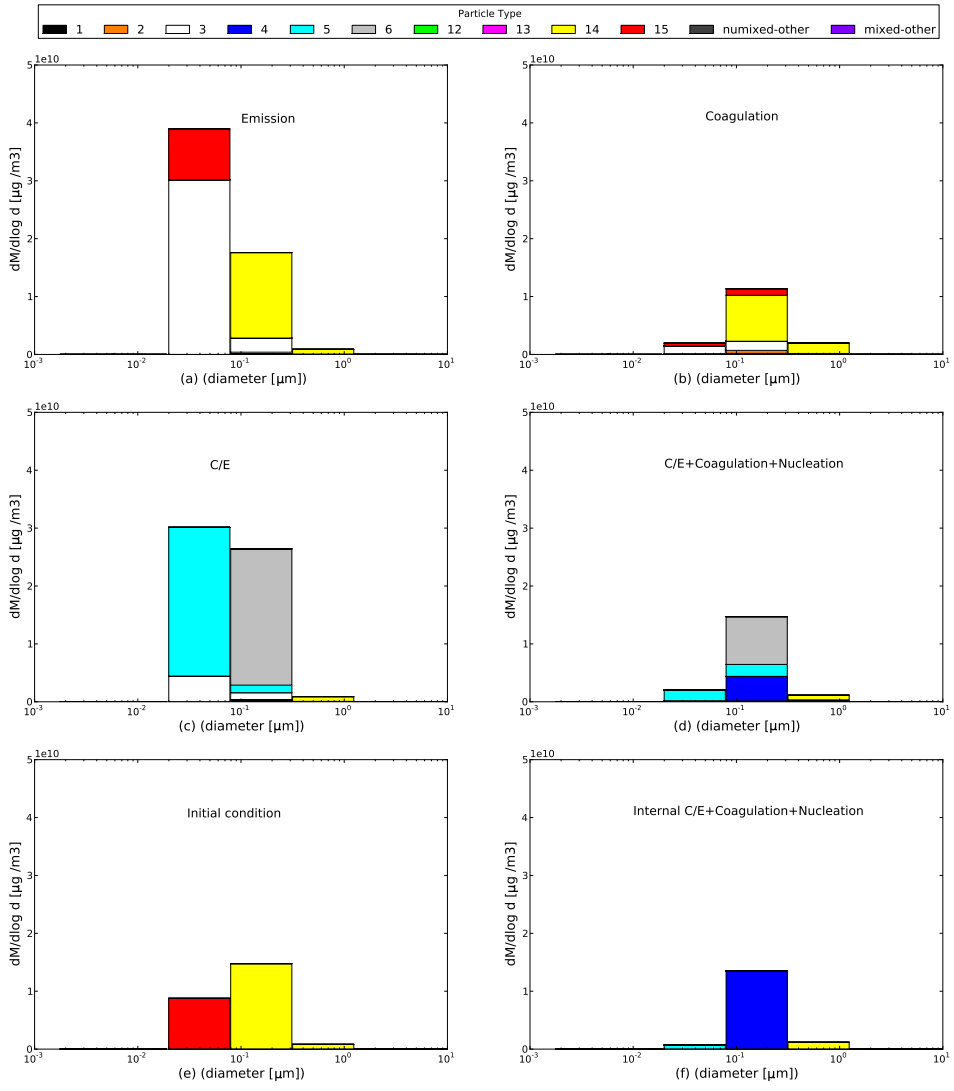

Figure 8. ~~Number~~ Result number distributions of externally-mixed particles as a function of particle diameter for the different chemical compositions for 6 different simulation scenarios: (a) Emission only; (b) Emission+Coagulation; (c) Emission+C/E; (d) Emission+Coagulation+C/E+nucleation; (e) Initial Condition; (f) Internal mixing result.

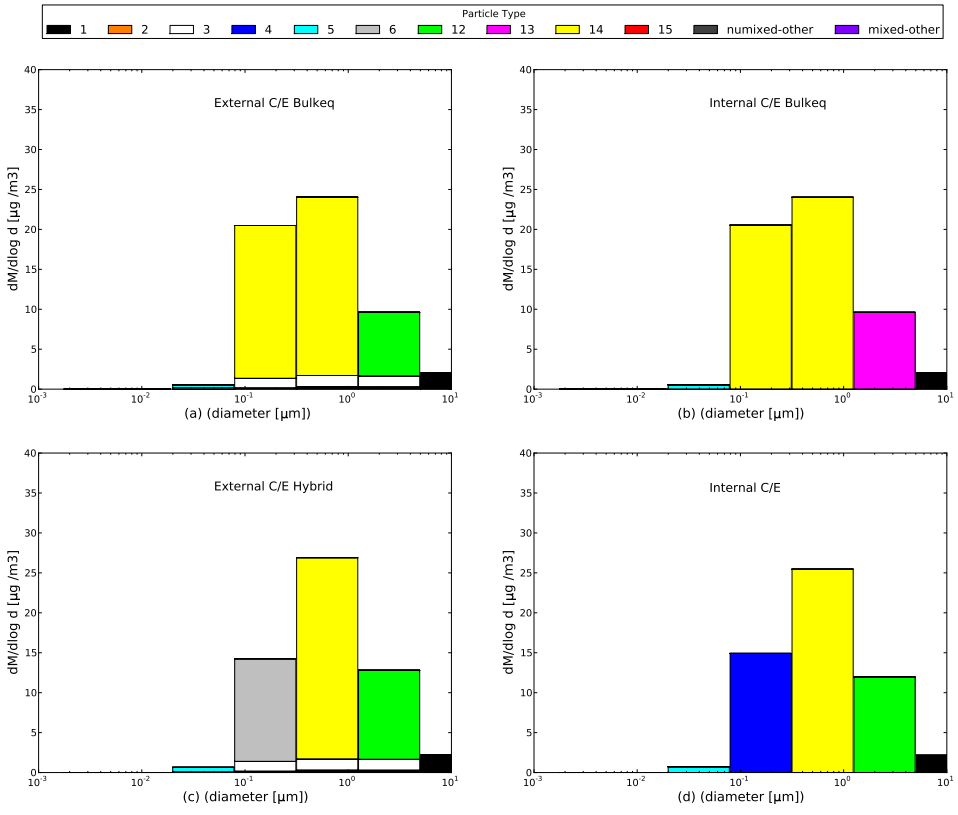

Figure 9. ~~Composition~~ Result mass distributions of externally-mixed ~~and internally-mixed~~ particles ~~: particle mass concentration~~ as a function of particle diameter for ~~particles of~~ the different chemical compositions for 4 different C/E simulation scenarios: (a) External bulk-equilibrium; (b) Internal bulk-equilibrium; (c) External hybrid method; (d) Internal dynamic.

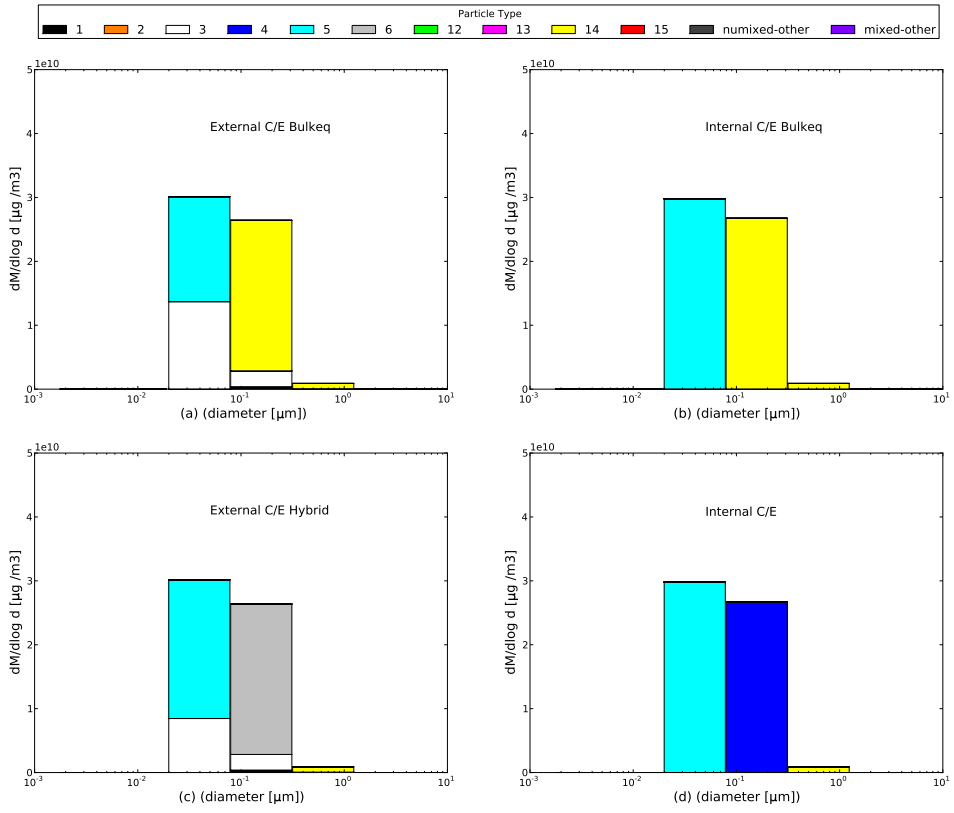

Figure 10. ~~Composition~~ Result number distributions of externally-mixed ~~and internally-mixed~~ particles ~~:~~ ~~particle number concentration~~ as a function of particle diameter for ~~particles of~~ the different chemical compositions for 4 different C/E simulation scenarios: (a) External bulk-equilibrium; (b) Internal bulk-equilibrium; (c) External hybrid method; (d) Internal dynamic.

Table 1. 20 Externally-mixed particle compositions

composition Index	Mixing state	Mass fraction of each groups (%)				
		HLI	HLO	HBO	BC	DU
1	unmixed(DU)	0-20	0-20	0-20	0-20	0-100
2	mixed	0-20	0-20	0-20	20-80	~~0-100~~0-80
3	unmixed(BC)	0-20	0-20	0-20	80-100	~~0-100~~0-20
4	mixed	0-20	0-20	20-80	0-20	~~0-100~~0-80
5	mixed	0-20	0-20	20-80	20-80	~~0-100~~0-60
6	unmixed(HBO)	0-20	0-20	80-100	0-20	~~0-100~~0-20
7	mixed	0-20	20-80	0-20	0-20	~~0-100~~0-80
8	mixed	0-20	20-80	0-20	20-80	~~0-100~~0-60
9	mixed	0-20	20-80	20-80	0-20	~~0-100~~0-60
10	mixed	0-20	20-80	20-80	20-80	~~0-100~~0-40
11	unmixed(HLO)	0-20	80-100	0-20	0-20	~~0-100~~0-20
12	mixed	20-80	0-20	0-20	0-20	~~0-100~~0-80
13	mixed	20-80	0-20	0-20	20-80	~~0-100~~0-60
14	mixed	20-80	0-20	20-80	0-20	~~0-100~~0-60
15	mixed	20-80	0-20	20-80	20-80	~~0-100~~0-40
16	mixed	20-80	20-80	0-20	0-20	~~0-100~~0-60
17	mixed	20-80	20-80	0-20	20-80	~~0-100~~0-40
18	mixed	20-80	20-80	20-80	0-20	~~0-100~~0-40
19	mixed	20-80	20-80	20-80	20-80	~~0-100~~0-20
20	unmixed(HLI)	80-100	0-20	0-20	0-20	~~0-100~~0-20

Table 2. Mixing state after 12hs simulation

Process	No Dynamic scenario (~~a~~A)	Coagulation scenario (~~b~~B)	C/E scenario (~~c~~C)	C/E+Coag+Nucl scenario (~~d~~D)
Mixed particle number (%)	42	79	48	51
Mixed particle mass (%)	83	85	64	76

Table 3. Computational times

Process	C/E	C/E bulk	C/E hybrid	Coag	C/E+Coag	C/E+Coag bulk	C/E+Coag hybrid
Internal mixing (s)	7.1	0.11	0.4	0.06	7.3	0.14	0.5
External mixing (s)	63.2	0.3	54.2	48.4	122.8	31.5	113